Research
A SCIENCE PARTNER JOURNAL

RESEARCH ARTICLE

A Study of Spontaneous Self-Injurious Behavior and Neuroimaging in Rhesus Macaques

Ya-Li Zhang[1,2†], Yi-Cheng Qiao[3,4†], Yun-Chao Ji[1,2,4†], Hong-Di Huang[1,2†], Long Zhang[1,2,4], Jian-Xiong Ruan[3,5], Chen-Yao Li[1,2,4], Hui-Heng Xie[1,2], Bao-Lin Zhang[1,6,7], Qi Zhou[8], Sha-Sha Yue[3], Xiao-Mei Yu[1,2], Ming-Hao Qiu[1,2], Chuan-Kai Yu[1,2], Si-Chu Wu[8], Yu-Fang Zhou[1], Yan-Ling Li[1], Hong-Mei Zhu[1], Shu-Zhen Dong[1], Kang Huang[9], Yun Wang[1], Qiong Wang[1], Yi-Jiang Li[1], Ya Xie[8], Hui-Ling Chen[1,2], Long-Bao Lv[1,2], Shu Liu[1,2,4,6], Yong-Gang Yao[1,2,4,6], Chun Wang[8*], Ning Liu[3,4*], and Jian-Hong Wang[1,2,4,6*]

[1]National Research Facility for Phenotypic & Genetic Analysis of Model Animals (Primate Facility) and National Resource Center for Non-Human Primates, Kunming Institute of Zoology, Chinese Academy of Sciences, Kunming, Yunnan 650107, China. [2]Yunnan Engineering Center on Brain Disease Models, Kunming Institute of Zoology, Chinese Academy of Sciences, Kunming 650107, China. [3]State Key Laboratory of Cognitive Science and Mental Health, Institute of Biophysics, Chinese Academy of Sciences, Beijing 100101, China. [4]College of Life Sciences, University of Chinese Academy of Sciences, Beijing 101408, China. [5]School of Life Sciences, Division of Life Sciences and Medicine, University of Science and Technology of China, Hefei, Anhui 230026, China. [6]State Key Laboratory of Genetic Evolution and Animal Models, Key Laboratory of Animal Models and Human Disease Mechanisms of Yunnan Province, and KIZ/CUHK Joint Laboratory of Bioresources and Molecular Research in Common Diseases, Kunming Institute of Zoology, Chinese Academy of Sciences, Kunming 650204, China. [7]Yunnan Key Laboratory of Biodiversity Information, Kunming Institute of Zoology, Chinese Academy of Sciences, Kunming, Yunnan 650201, China. [8]The Affiliated Brain Hospital of Nanjing Medical University, Nanjing, China. [9]Guangdong Bayone Biotech CO., Ltd., Guangzhou, China.

*Address correspondence to: wangjh@mail.kiz.ac.cn (J.-H.W.); liuning@ibp.ac.cn (N.L.); chun_wang@njmu.edu.cn (C.W.)
†These authors contributed equally to this work.

Nonsuicidal self-injury (NSSI) demonstrates escalating prevalence among adolescents as a maladaptive behavior characterized by deliberate self-harm, yet its neurobiological underpinnings remain elusive. Spontaneous self-injurious behavior (SIB) in nonhuman primates (NHPs) emerges as a clinically relevant animal model for investigating NSSI pathogenesis and therapeutic interventions. However, previous studies have yet to comprehensively evaluate the translational value of self-injury in NHPs through integrated behavioral and neuroimaging characterization. In this study, we identified spontaneously self-injurious macaques within our NHP colony and performed multimodal assessments encompassing ethological profiling, neuroendocrine assays, metabolomic analysis, and neuroimaging. Our results revealed that SIB macaques exhibited biological patterns and temporal onset sequences of self-harm, accompanied by a locomotor and social interaction decrease based on 3-dimensional deep-learning recognition, sensory processing deficits, and impairments in emotional and cognitive processing. Biochemical profiling demonstrated reduced plasma concentrations of cortisol, serotonin, and oxytocin, coupled with metabolomic disturbances including up-regulation of digestive-related pathways and down-regulation of dopaminergic synaptic signaling and phosphatidylinositol metabolism. Neuroimaging analyses identified structural abnormalities featuring volumetric enlargement in amygdala and midbrain regions alongside gray matter reduction in the frontal and parietal lobes. Enhanced structural and functional connectivity was observed. Network-based statistics highlighted increased functional connectivity primarily between the frontal and parietal lobes. These alterations demonstrated a partial correlation with observed behavioral deficits in the self-injury macaques. Notably, a series of administration of low-dose ketamine had no effect on SIB and the physical index. Our integrative multi-omic approach elucidates the neurobiological phenotype of spontaneous SIB in macaques, highlighting the value of the SIB model for pathogenetic investigation and therapeutic development in human NSSIs.

Citation: Zhang Y-L, Qiao Y-C, Ji Y-C, Huang H-D, Zhang L, Ruan J-X, Li C-Y, Xie H-H, Zhang B-L, Zhou Q, et al. A Study of Spontaneous Self-Injurious Behavior and Neuroimaging in Rhesus Macaques. *Research* 2025;8:Article 0782. https://doi.org/10.34133/research.0782

Submitted 1 March 2025
Revised 17 June 2025
Accepted 23 June 2025
Published 31 July 2025

Introduction

Nonsuicidal self-injury (NSSI) disorder, classified as a distinct clinical condition in *Diagnostic and Statistical Manual of Mental Disorders—Fifth Edition* (DSM-5), involves deliberate self-harm without suicidal intent, often manifesting as cutting, burning, or hitting to induce pain or tissue damage. Prevalence ranges from 1% to 4% in adults to 15% to 18% in adolescents, with underdiagnosis potentially elevating real-world rates [1,2]. Triggered by emotional distress or interpersonal conflicts, NSSI individuals may exhibit functional heterogeneity across emotional regulation, attention-seeking, and social avoidance [3]. DSM-5 criteria specify that NSSI behaviors aim to (a) alleviate negative emotions/cognitions, (b) resolve relational difficulties, or (c) generate positive feelings. In addition, NSSI shows heterogenetic traits, e.g., intellectual disability, aggression, and impulsivity, and frequently co-occurs with borderline personality disorder, major depressive disorders, eating disorders, and substance disorders or none [1,4]. Alarmingly, NSSI populations face elevated suicide risks despite the nonsuicidal intent [5].

NSSI arises from multifactorial etiopathogenesis involving stress-response dysfunction, genetic susceptibility, and environmental triggers. Blunted hypothalamic–pituitary–adrenal (HPA) axis activity and epigenetic glucocorticoid receptor dysregulation contribute to stress hypersensitivity, aggression, and social/sleep impairments [6]. While genome-wide studies identify suicide-related risk genes [7], specific NSSI-associated genetic markers remain undefined.

NSSI remains poorly understood, hampered by limited animal models. Valid models of self-injurious behavior (SIB) are critical for identifying the pathogenesis, therapeutic targets, and biomarkers of NSSI. Current rodent models primarily utilize monoamine agonists (e.g., pemoline) or anxiety-inducing agents (e.g., FG 7142) to induce SIB yet lack spontaneous occurrence (<5% prevalence) and human-relevant complexity in social–emotional expression [8]. These pharmacological interventions also limit translational relevance to human NSSI. Nonhuman primates (NHPs), particularly Old World macaques, offer unique advantages with 11%–15% to 1%–5% spontaneous SIB rates in captivity as the condition improved [6]. Their self-injury patterns, including limb biting, head-banging, and hair-pulling, mimic human NSSI in both behavioral topography (skin wounds and tissue damage) and severity gradation. Crucially, macaques share >93% genetic homology with humans and possess homologous prefrontal cortical structures essential for emotion regulation and social cognition. This neuroanatomical fidelity enables the investigation of stress-axis dysregulation (e.g., HPA hyperactivity) and epigenetic mechanisms implicated in SIB. While genome-wide studies in rodents identify candidate pathways, NHP models uniquely capture the interplay between intrinsic vulnerabilities (genetic/epigenetic) and environmental stressors that may drive spontaneous SIB. Their complex social hierarchies and emotional repertoires permit ecologically valid studies of trigger contexts (e.g., social conflict and anxiety) absent in rodent paradigms. By bridging molecular mechanisms with clinically relevant phenotypes, NHP models may hold unparalleled potential for advancing NSSI research and therapeutic development.

This study established a novel translational framework for NSSI research by identifying spontaneously self-injurious macaques within our NHP colony. A comprehensive behavioral battery assessed locomotor patterns, social interaction, exploratory behavior, emotional and defensive responses, spatial working memory (SWM), and cognitive flexibility to map phenotypic parallels with human NSSI. We further characterized the biological rhythm and behavioral sequencing of SIB. Multimodal biomarkers were investigated through cerebrospinal fluid (CSF) metabolomics, plasma hormonal levels, structural magnetic resonance imaging (MRI), and resting-state functional MRI (rs-fMRI). Therapeutic potential was evaluated via low-dose ketamine intervention. This work provides a valid NHP model of spontaneous SIB mirroring core NSSI features and a multi-omic platform for mechanistic discovery and therapeutic development.

Results

Characterization of self-injury macaques

Self-injured wounds were found in self-injury macaques' limbs reflected by mean wound scores between 3 and 58 when tested at different times. The video recordings of 10 self-injury macaques revealed that 5 of the macaques exhibited hysterical clusters of hand-biting, while the other 5 demonstrated leg-biting. The SIB occurred in the form of clusters, with the macaques repetitively engaging in self-biting. On average, a single episode of SIB lasted for 1.50 ± 0.22 s.

We found that the macaques' SIB demonstrated sequential traits (Table). It manifested as several episodes where the macaques were mostly quiet, followed by repetitive hysterical self-biting that appeared as clusters of SIB onsets. Eventually, it ended with the macaques being mostly quiet (Movie S1) or engaging in stereotypical behavior (Movie S2) after one or several clusters of SIB. This suggested that the macaques' SIB might be driven by impulsivity, and it seemed that the macaques experienced relief from repetitive self-injury, lending support to the hypothesis that SIB is a form of sensation seeking in response to impoverished environments [6]. It was observed that 10% aggression occurred prior to the onset of SIB, indicating that a few macaques might redirect threatening behavior toward themselves, as mentioned by Novak and Meyer [6].

The macaques with SIB exhibited a tendency to have a lower 3-dimensional (3D) movement speed of main body parts (head, neck, shoulder, limbs, knees, etc.) within 35 min (Fig. 1A and B). Analysis of the behavior patterns showed a significantly

Table. The sequential behavior of self-injury

Behavior	SIB	Prior to SIB	Post-SIB
Sitting or standing while observing outside	Single	32.61%	43.75%
	Cluster	30.00%	40.00%
Observing the self-bitten site	Single	26.09%	6.25%
	Cluster	20.00%	0.00%
Stereotypical circling	Single	21.74%	29.17%
	Cluster	20.00%	40.00%
Aggressively shaking the cage or opening the mouth	Single	15.22%	6.25%
	Cluster	10.00%	10.00%
Other behaviors (grooming or scratching head)	Single	4.35%	14.58%
	Cluster	20.00%	10.00%

SIB, self-injurious behavior

more sitting behavior in non-apparent displacement than the controls ($P = 0.034$) (Fig. 1C). Self-injury macaques showed overall low axial diffusivity (AD) and high non-apparent displacement when compared with the controls (Fig. S1A). Principal component analysis of kinematic parameters showed that the self-injury macaques exhibited relatively concentrated

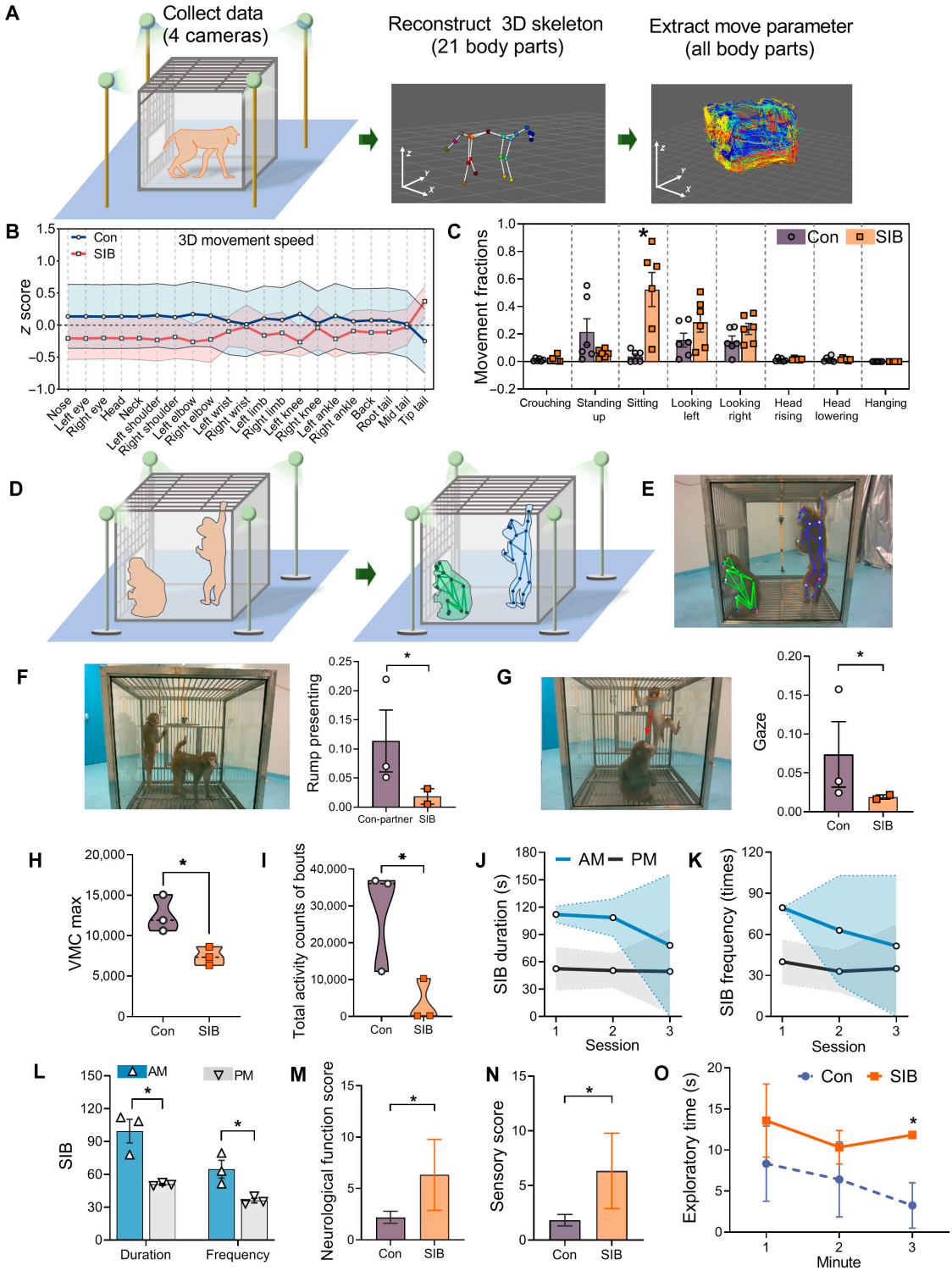

Fig. 1. The behavioral experiments in macaques. (A) Schematic diagram of the testing dynamics of spontaneous behavior in macaques. (B and C) Comparison of movement speeds (B) and behavioral postures (C) between SIB and control macaques using 3-dimensional (3D) deep-learning-based recognition. (D) Schematic diagram of paired social interaction test. (E) Photo showing the identified macaques. (F) Macaque rump presenting and fractions between the control partner and SIB groups. (G) Macaque gaze and fractions between the control and SIB groups. The red line illustrates the macaque's gazing direction. (H and I) Quantified using ActiGraph. Maximum vector magnitude counts (VMCs) (H) and total activity counts of bouts (I) per hour. (J to L) Duration and frequency of SIB measured in the morning (AM) and afternoon (PM). (M and N) Scores of total neurological function (M) and sensory function (N). (O) Exploratory behavior in the macaques. Data are expressed as mean ± standard error of the mean (SEM). *$P < 0.05$; self-injury macaques (SIB) vs. the controls (Con) or AM vs. PM.

values along the first principal component (PC1) and second principal component (PC2), whereas the control animals displayed a broader range of individual variability (Fig. S1B). In the paired social interaction test (Fig. 1D and E), 2 self-injury macaques showed lower social interaction, reflected by significantly lower fractions of rump presenting ($P = 0.023$, Fig. 1F) and gaze ($P = 0.037$, Fig. 1G) to the other when compared with control partners and controls, respectively. No significant differences were found in approaching behavior. The daily activity from the ActiGraph showed that the self-injury macaques exhibited a lower level of daily locomotor activity, reflected by a significantly lower maximum vector magnitude counts than the controls ($P = 0.03$) and lower activity counts of bouts per hour ($P = 0.04$) (Fig. 1H and I). These results were consistent with previous reports where low levels of physical activity were observed in individuals with NSSIs [9].

The macaques exhibited a biological rhythm with more seizures occurring in the morning; the duration and frequency (Fig. 1J and K) of SIB tended to decrease as testing sessions increased, suggesting a slight habituation. Moreover, SIB showed a longer duration ($P = 0.011$) and a higher frequency of SIB ($P = 0.027$) in the morning than in the afternoon (Fig. 1L). It was similar to clinical studies indicating that diurnal rhythms modulated various pathophysiology and neurological disorders such as epilepsy [10].

The self-injury macaques had a serious disruptive neurological function compared with a large number of controls ($P = 0.042$, $n = 18$, Fig. 1M), and this difference was reflected by the impaired sensory function ($P = 0.021$, Fig. 1N), which mainly included the pain sensitivity test. The decreased pain sensitivity may contribute to the induction of repetitive SIB both in animals and in human NSSIs [11]. The self-injury macaques showed a longer duration of exploration to the moving laser icon than the controls (on the third minute, $P = 0.038$, Fig. 1O), suggesting that the SIB macaques had an abnormal nature exploratory behavior, probably due to sensory dysfunction.

Macaques with SIB showed abnormal emotional responses

We tested the emotional responses of macaques when being challenged with different stimuli (Fig. 2A). The self-injury macaques showed quicker habituation to the rubber snake and similar habituation to neutral stimuli as the controls (Fig. 2B). Moreover, the self-injury macaques failed to show significant difference in latency (Fig. 2C) or reward retrieval (Fig. 2D) among stimuli, suggesting deficits of defensive behavior and emotional processing when compared with the control animals showing significant difference between the rubber snake and other stimuli (longer latency facing the rubber snake than facing the rubber spider [$P < 0.001$], neutral [$P = 0.001$], and null [$P < 0.001$]; took more food when the spider [$P < 0.001$], neutral [$P = 0.001$], and null [$P < 0.001$] rather the rubber snake was presented).

Similarly, in the human intruder test (Fig. 2E), macaques with SIB stayed in front of the cage for a significantly longer time than the controls at no eye contact (NEC) conditions ($P = 0.041$) (Fig. 2F), showed a higher frequency of self-directed (biting) behavior than control macaques at NEC ($P = 0.05$) conditions (Fig. 2G). However, self-injury macaques showed a tendency to have lower vigilance (Fig. 2H), threatening (Fig. 2I), and locomotor activity (Fig. 2J) depending on the position of the intruder, when compared with the control group. These results demonstrated less defensive and less anxious responses to the human intruder in the self-injury macaques.

Macaques with SIB presented impaired SWM

When the macaques were trained in the SWM task (Fig. 3A), macaques with SIB needed more sessions to obtain the criterion at $B = 0$ s than controls ($P = 0.001$) (Fig. 3B). The fast learner control macaque spent 7 sessions to obtain the criterion when $B = 0$ s. Thus, we analyzed the performance of 7 sessions between 2 groups and found a significantly lower percentage of correct choices in self-injury macaques than controls at session 5 ($P = 0.035$), session 6 ($P = 0.05$), and session 7 ($P = 0.015$) (Fig. 3C). When $B = 3$ s (Fig. 3D), the performance decreased as the delay time increased (overall delay time effect $F(5,20) = 15.09$, $P < 0.001$), and this decrease was significantly faster in self-injury macaques (interaction of group × delay time $F(5,20) = 5.21$, $P = 0.003$; between-group effect $F(1,4) = 17.01$, $P = 0.015$). The correct choices were significantly lower in SIB than in controls at delay times of 3 s ($P = 0.034$), 6 s ($P = 0.024$), 9 s ($P = 0.021$), 12 s ($P = 0.005$), and 15 s ($P = 0.028$).

In the reversal learning (RL) task (Fig. 3E), 2 self-injury macaques failed to obtain the criterion at the acquisition of discrimination training, resulting in a significantly higher number of sessions in the SIB group than in the control group ($P = 0.041$, Fig. 3F and G). After the reward was reversed from the solid cycle into the diamond, the macaques gradually learned the new rule (overall session effect $F(19,38) = 23.51$, $P < 0.001$), and this learning was significantly slower in self-injury macaques (interaction of group × session $F(19,38) = 7.10$, $P < 0.001$). The self-injury macaques failed to obtain the criterion (Fig. 3H). As shown in Fig. 3I, significantly lower performances were found in the SIB group than in controls at session 12 ($P = 0.004$), session 13 ($P = 0.001$), session 14 ($P = 0.03$), session 15 ($P = 0.011$), and session 16 ($P = 0.016$). These findings were consistent with previous studies indicating that cognitive risk factors have associations with the functions and severity of SIB in the macaque model and NSSI [12,13]. However, the SIB group showed a higher performance than controls at session 1 ($P = 0.004$) when the reward was reversed, suggesting an abnormal behavior.

Similarly, we measured the bias score, which may reflect a stereotypical behavior, and the switch score in the win–stay–lose–shift paradigm [14], which may represent impulsivity, and found self-injury macaques significantly increased the bias to choose one side after the reward stimulus shifted to the opposite of the previous rule ($P = 0.039$, as shown in Fig. 3J) although there was no significant difference in bias score between SIB and control macaques during the acquisition. Moreover, the self-injury macaques showed a significantly higher percentage of win–shift and lose–shift than the controls during the RL process ($P = 0.0002$) (Fig. 3K). In detail, the self-injury macaques presented a significantly lower percentage of win–stay ($P = 0.025$) and a higher percentage of win–shift ($P = 0.0004$), and also a tendency toward a shorter reaction time, when compared with the controls (Fig. 3L). These findings were consistent with the pathogenesis hypothesis that compulsivity and impulsivity might be an implicit cause of SIB, which has also been observed in NSSI [15].

Self-injury macaques showed lower levels of cortisol, serotonin, and oxytocin in plasma and dysregulated metabolomic patterns in CSF

Considering the impact of hormones on SIB, the emotion-related hormones in peripheral circulation were measured. The self-injury macaques had significantly lower cortisol ($P = 0.003$) and serotonin (5-HT) ($P = 0.046$) and a trend

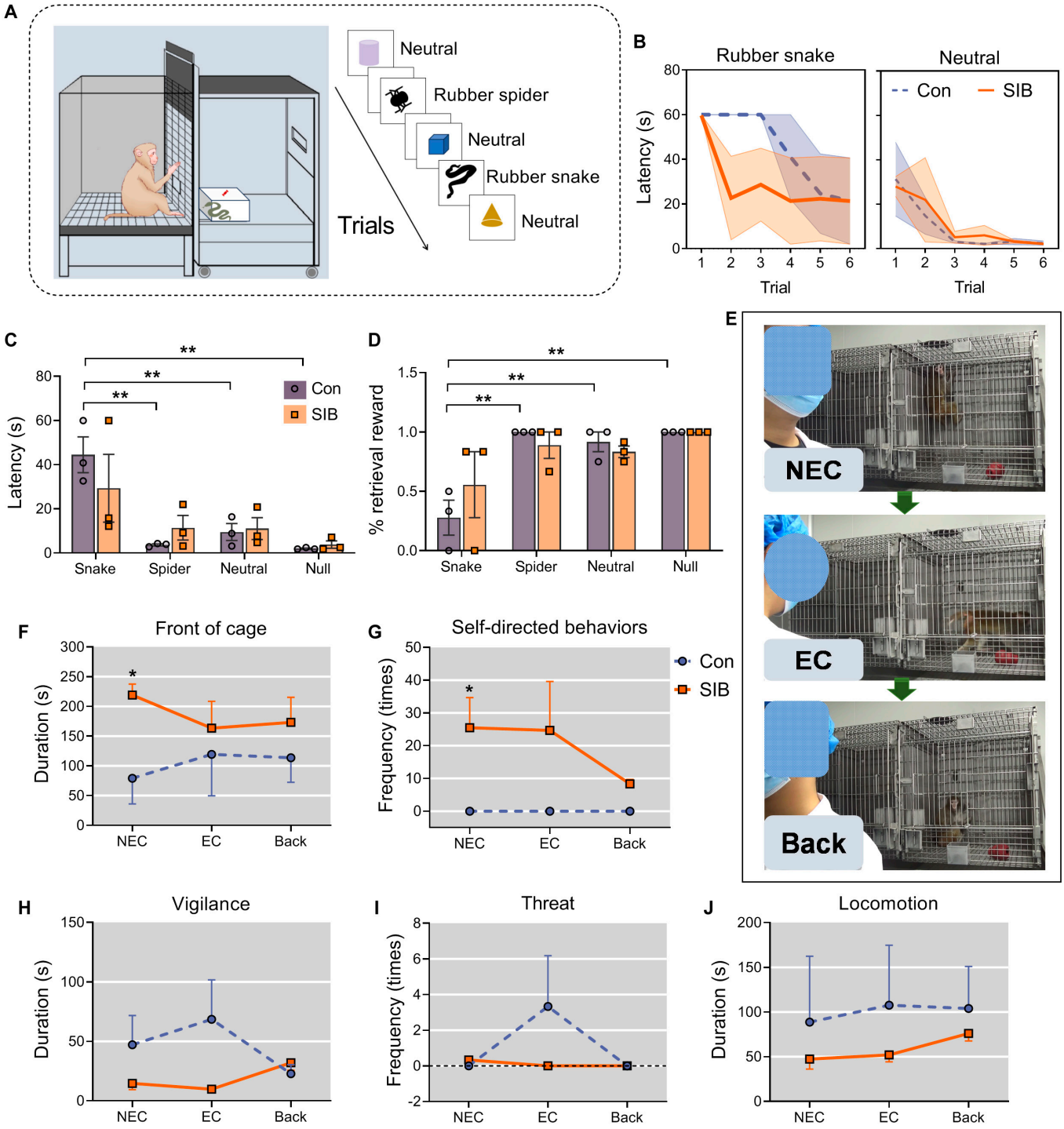

Fig. 2. The emotional/defensive response tests in macaques. (A) Schematic diagram of emotional response test. (B to D) Behavioral results of emotional response test. The macaques with SIB tended to have a faster habituation to the rubber snake when compared with the control, and both groups showed a similar habituation to neutral stimuli (B). The latency (C) and percentage (D) for the macaques taking food rewards under different stimuli (**$P < 0.01$, rubber snake vs. rubber spider, neutral or null). (E) Schematic diagram of the defensive response test in the human intruder test (HIT) under 3 conditions: no eye contact (NEC), eye contact (EC), and back. (F to J) Behavioral results of HIT under different conditions. Self-injury macaques showed lower defensive behaviors, reflected by a longer-duration stay in front of the cage (F), higher self-directed (self-biting) behavior (G), a trend of lower vigilance (H), lower threat (I), and lower locomotor activity (J) when compared with the controls. Data are expressed as mean ± SEM. *$P < 0.05$ and **$P < 0.01$, self-injury macaques (SIB, $n = 3$) vs. the controls (Con, $n = 3$).

toward lower oxytocin in the plasma when compared with the control animals (Fig. 4A to C), which were partly consistent with the findings of clinical and animal studies [6,16,17].

Furthermore, metabolomic analysis showed that 969 metabolites had been determined in the macaques. We identified a total of 30 differential metabolites between the SIB and control groups, including 20 down-regulated metabolites, such as myo-inositol and arachidic acid, and 10 up-regulated metabolites, including phosphatidylcholine, triglycerides, and diacylglycerol (Fig. 4D). In detail, 9 differential metabolites were hydrophilic

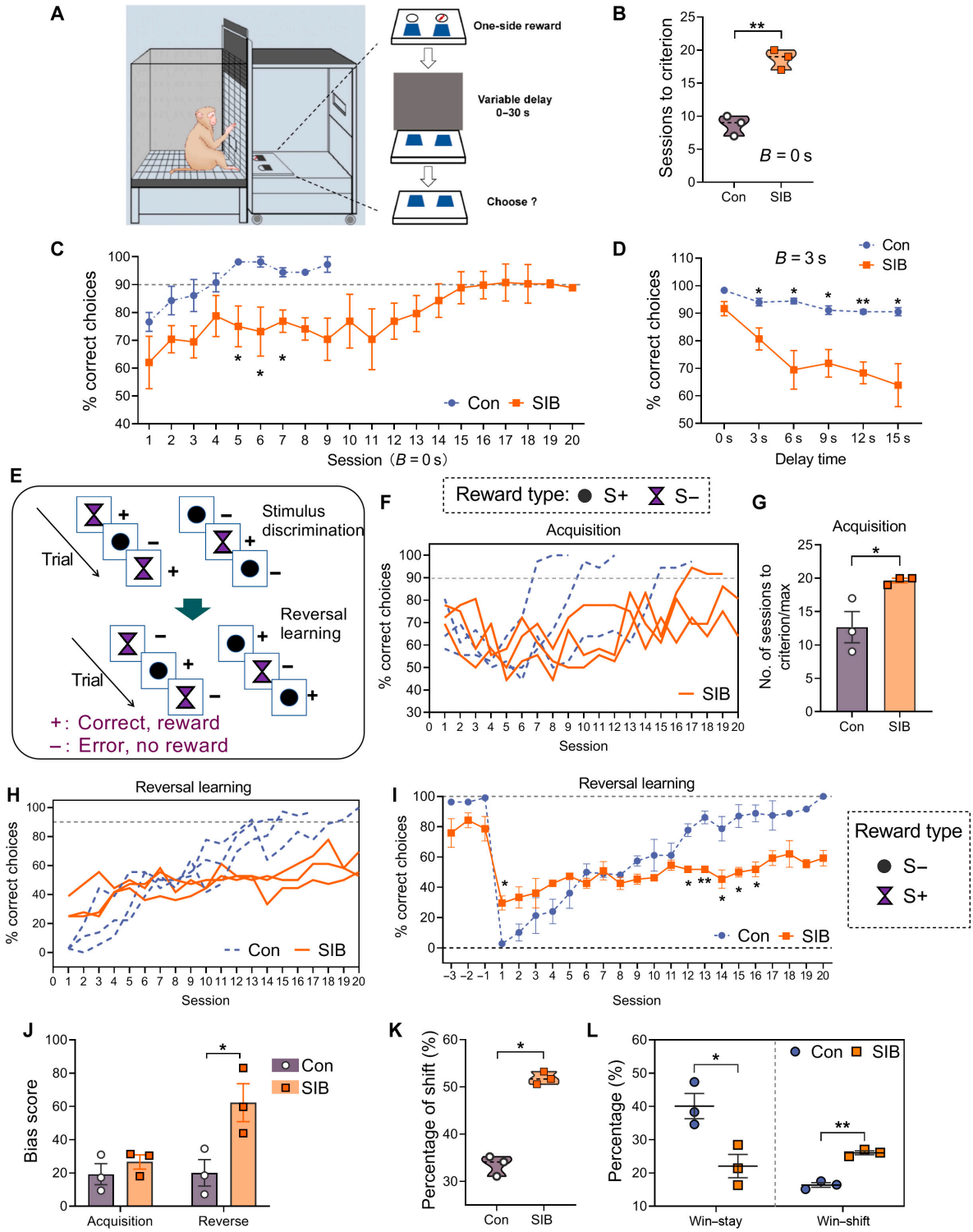

Fig. 3. The cognitive experiments in macaques. (A) Schematic diagram of the spatial working memory (SWM) task [23]. (B and C) Results of the SWM test at $B = 0$ s. Macaques with SIB needed more sessions to obtain the criterion (B) and performed a lower percentage of correct choices than controls depending on the session (C). (D) SIB macaques showed lower performance across the delay time than controls at $B = 3$ s. (E) Schematic diagram of the reversal learning (RL) task. (F and G) Percentage of correct choices across sessions (F) and the numbers of sessions to obtain the criterion (G) during the acquisition stage. (H and I) Percentage of correct choices in the RL task. The dotted line in (C), (F), and (H) shows the criterion. (J) The bias scores in SIB and control macaques during the acquisition and RL. (K) Percentage of shifting during the RL stage. (L) Self-injury macaques showed a significantly lower percentage of win–stay and a higher percentage of win–shift than the controls. Data are expressed as mean ± SEM. $^*P < 0.05$ and $^{**}P < 0.01$, self-injury macaques. SIB, $n = 3$; Con, $n = 3$.

metabolites and the other 21 differential metabolites were lipids (Tables S1 and S2). We next performed Kyoto Encyclopedia of Genes and Genomes pathway enrichment analysis and calculated the differential abundance scores of differential pathways separately on CSF hydrophilic metabolites and lipids. Results showed that pathways related to carbohydrate

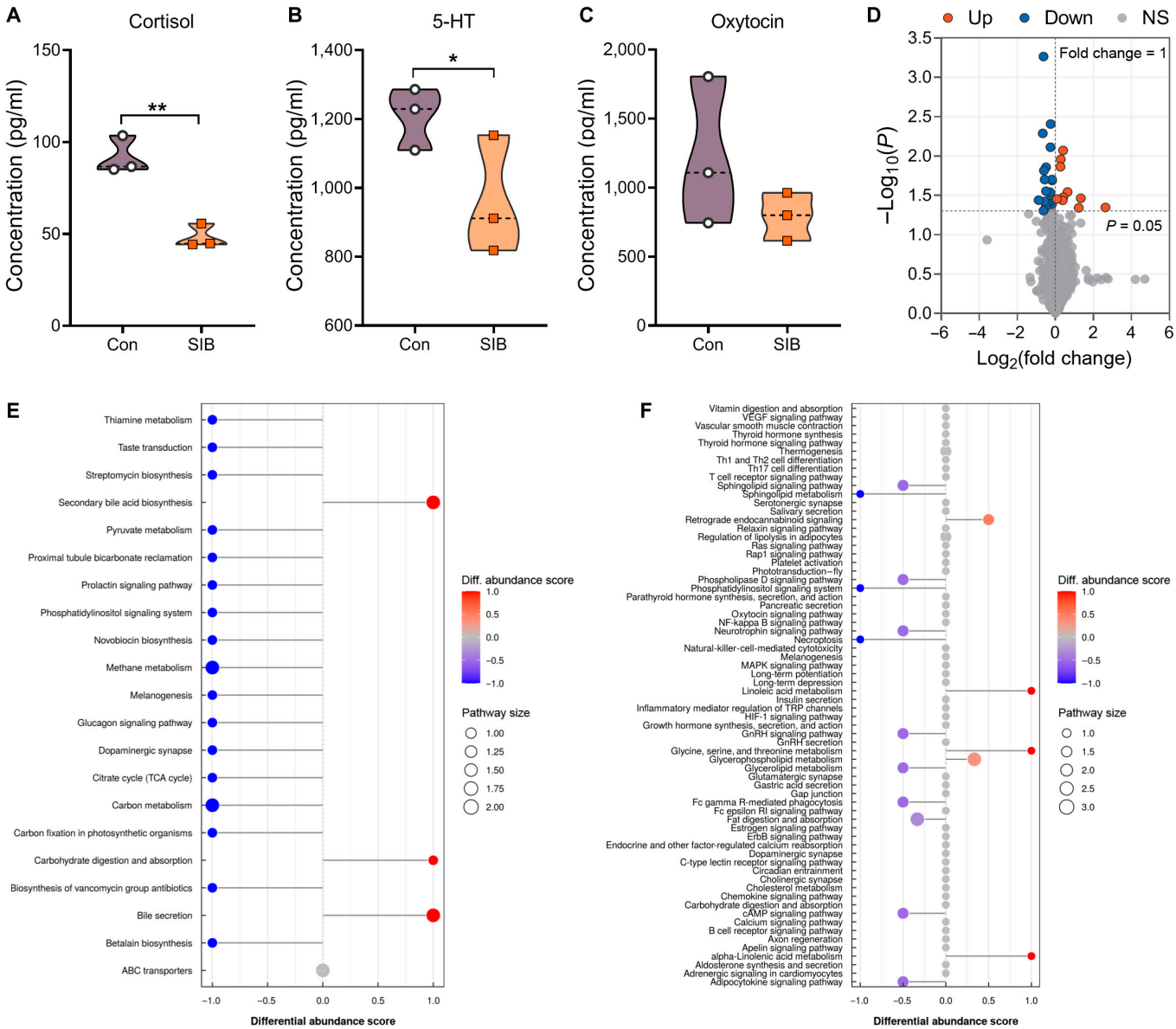

Fig. 4. The plasma hormone level and cerebrospinal fluid (CSF) metabolomic pattern in macaques. (A to C) Plasma concentrations of cortisol, serotonin (5-HT), and oxytocin in SIB macaques versus controls. (D) Volcano plot illustrating the metabolites with significant differences. Up (red dots), up-regulation; Down (blue dots), down-regulation; NS (gray dots), no significant difference. (E and F) Plots showing the differential abundance score of differential Kyoto Encyclopedia of Genes and Genomes (KEGG) pathways in hydrophilic metabolites (E) and lipids (F) in CSF. Data are expressed as mean ± SEM. *$P < 0.05$; **$P < 0.01$. SIB, $n = 3$; Con, $n = 3$.

digestion were notably up-regulated; however, dopaminergic synapse activity and the phosphatidylinositol signaling pathway were significantly down-regulated in self-injury macaques when compared with those of the controls.

Self-injury macaques had significant brain structural changes compared with control macaques

We used a general linear mixed model (GLMM) to compare the subcortical volumes of macaques exhibiting SIB with those of the controls. Our analysis revealed that the self-injury macaques had significantly larger subcortical volumes than the controls ($P = 0.002$) (Fig. 5A). To pinpoint which specific subcortical structures contributed to this overall difference, we performed GLMM analyses on 13 defined subcortical structures. We found that 5 of these structures were significantly larger in the self-injury macaques than in the controls (uncorrected $P < 0.05$), including the amygdala ($P = 0.002$), the midbrain ($P = 0.002$), lateral and ventral pallium ($P = 0.038$), pallidum (uncorrected $P = 0.024$), and pretectum (uncorrected $P = 0.029$) (Fig. 5B). Additionally, the ventricles were significantly enlarged in self-injury macaques compared with those in the control animals ($P < 0.001$) (Fig. 5C).

We employed a GLMM to compare gray matter volumes (GMVs) between SIB and control macaques. Our analysis revealed a significant reduction in whole-brain GMV in the self-injury macaques ($P = 0.010$) (Fig. 5D). To gain a deeper understanding of GMV changes in self-injury macaques, we divided the cortical surfaces into 4 lobes and 88 regions using the CHARM1 and CHARM5 templates. Our analysis revealed significant reductions in GMV in both the frontal lobe ($P = 0.017$) and the parietal lobe (uncorrected $P = 0.035$) (Fig. 5E). Within the frontal lobe, notable decreases were observed in the

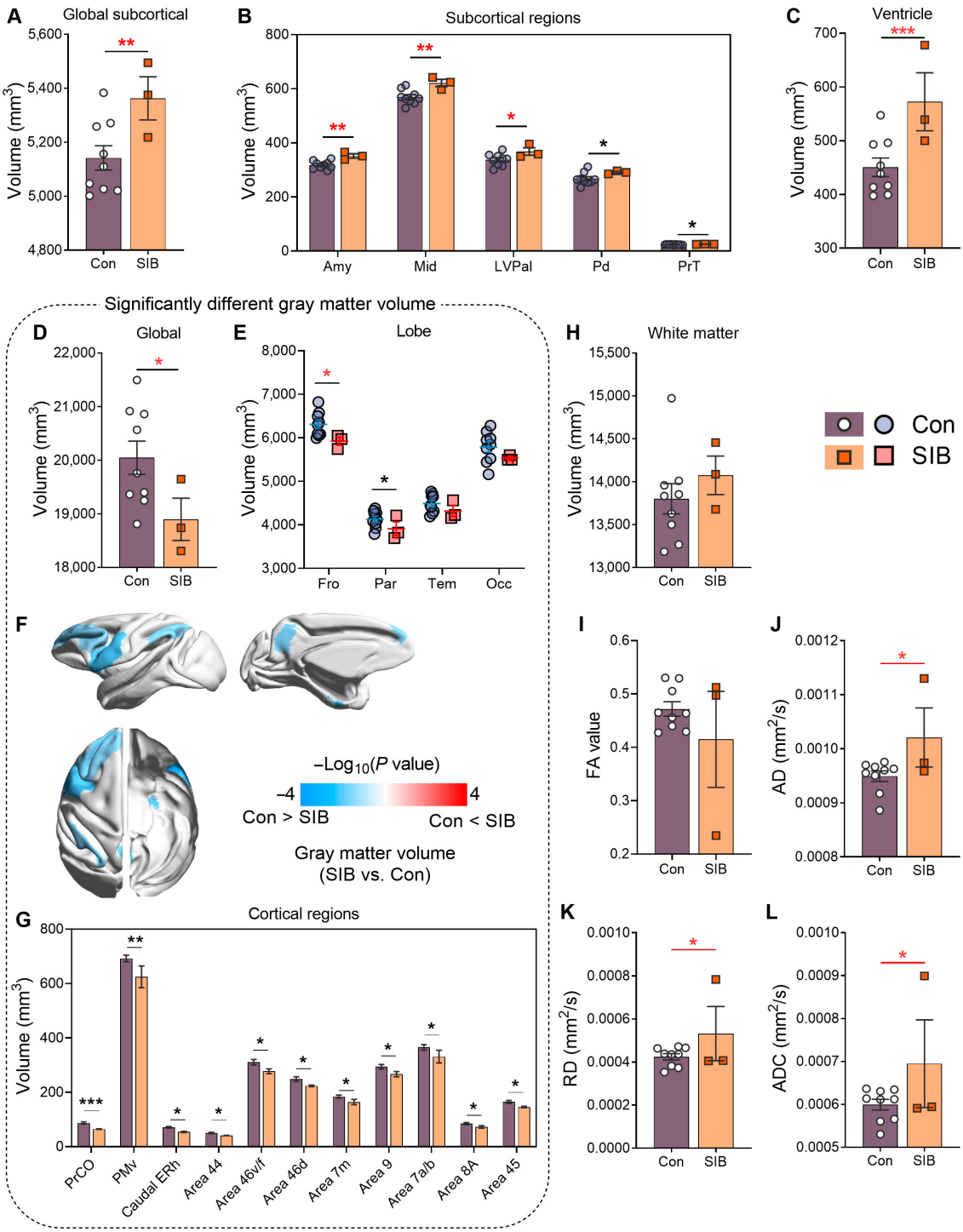

Fig. 5. Differences in brain structure between SIB macaques and controls. (A to C) Volume of subcortical structures (A), detailing subcortical regions (B) and ventricle (C) with significant differences between SIB and control macaques. Amy, amygdala; Mid, midbrain; LVPal, lateral and ventral pallia; Pd, pallidum; PrT, pretectum. (D and E) Gray matter volume (GMV) at the whole-brain level (D) and the lobe level (E). Fro, frontal lobe; Par, parietal lobe; Tem, temporal lobe; Occ, occipital lobe. (F) Visualization of the cortical regions in (G) on the mid-gray surfaces of the macaque template. Red indicates regions where self-injury macaques had a larger GMV than controls, while blue indicates the opposite. (G) The GMV in cortical regions with significant differences between macaques with SIB and controls. PrCO, precentral operculum; PMv, ventral premotor cortex. (H to L) Bar plots representing the volume (H), fractional anisotropy (FA) (I), axial diffusivity (AD) (J), radial diffusivity (RD) (K), and apparent diffusion coefficient (ADC) (L) of white matter (WM) at the whole-brain level in self-injury macaques versus controls. *$P < 0.05$; **$P < 0.01$; ***$P < 0.001$; red asterisks indicate false discovery rate (FDR)-corrected P values: *$P < 0.05$; **$P < 0.01$; ***$P < 0.001$. SIB, $n = 3$; Con, $n = 9$.

ventrolateral prefrontal cortex (PFC) across area 44 (uncorrected $P = 0.011$), area 46v/f (uncorrected $P = 0.022$), and area 45 (uncorrected $P = 0.050$); the dorsolateral PFC in area 46d (uncorrected $P = 0.028$) and area 9 (uncorrected $P = 0.041$); the orbitofrontal cortex (OFC) at the precentral operculum (uncorrected $P < 0.001$); the frontal eye field area 8A (uncorrected $P = 0.050$); and the motor cortex at the ventral premotor cortex (uncorrected $P = 0.008$). In addition, we identified

significant volume reductions in the temporal lobe at the caudal entorhinal cortex (ERh) (uncorrected $P = 0.011$) and in the parietal lobe at areas 7m (uncorrected $P = 0.031$) and 7a/b (uncorrected $P = 0.041$) (Fig. 5F and G).

We also quantified potential changes in white matter (WM) in macaques with SIB, but we did not find significant differences in WM volume between the SIB and the control group ($P = 0.243$, Fig. 5H). However, we indeed observed significantly higher values in the self-injury macaques for the diffusion tensor imaging scalar metrics: AD ($P = 0.014$), radial diffusivity ($P = 0.035$), and apparent diffusion coefficient ($P = 0.026$) (Fig. 5I to L). These results suggest potential microstructural changes in the WM of the self-injury macaques.

Macaques with SIB showed enhancement of structural connectivity and functional connectivity

The whole-brain structural connectivity (SC) strength in the SIB group exhibited an increasing trend ($P = 0.259$) relative to that in controls (Fig. 6A). At the lobar level, we found that the self-injury macaques exhibited stronger SC between most lobes (Fig. 6C). Notably, the SCs between the parietal and occipital lobes ($P = 0.001$) and between the frontal lobe and subcortical structures ($P = 0.005$) were significantly stronger in the SIB group (Fig. 6B).

We then conducted a region-based analysis on 101 predefined brain regions, comprising 88 cortical and 13 subcortical regions in each hemisphere. Regions with a higher SC strength in the self-injury macaques were primarily located in multimodal areas such as the medial OFC, temporal pole, and parietal lobe: area 25 ($P = 0.001$), fundus intraparietal sulcus ($P = 0.029$), ERh ($P = 0.029$), granular temporal pole ($P = 0.029$), and floor of the superior temporal area ($P = 0.029$). Additionally, 12 cortical regions in the self-injury macaques exhibited a significantly higher SC strength compared with those in the control group, albeit to a lesser extent (Fig. 6D and E, uncorrected $P < 0.05$). Conversely, only 2 subcortical regions in the SIB group demonstrated reduced SC strength (uncorrected $P < 0.05$).

Using network-based statistics (NBS), we identified 79 brain region-to-region connections that were significantly stronger in the SIB than in the control macaques (shown as red lines in Fig. S2A) and 27 connections that were significantly weaker (shown as blue lines in Fig. S2A). The stronger connections in the self-injury macaques compared with those in the controls were primarily concentrated within the frontal and temporal lobes, as well as between these lobes and subcortical structures (Fig. S2B). In contrast, the weaker connections in the SIB group were mainly located between the parietal and temporal lobes (Fig. S2C).

We employed a series of GLMMs to conduct a comparative analysis of rs-fMRI between the SIB and the control macaques at 3 levels: whole brain, lobe, and specific brain regions. We calculated whole-brain mean functional connectivity (FC) as the average value of the lower triangle of the FC matrix. Our results indicated a trend toward increased mean FC in self-injury macaques, although this was not statistically significant ($P = 0.084$, Fig. 6F). Further analyses of FC differences among the 4 lobes (frontal, parietal, temporal, and occipital) and subcortical structures showed higher FC values in self-injury macaques compared with those in controls, which aligns with the observed enhancement at the whole-brain level (Fig. 6H). Specifically, self-injury macaques exhibited significantly higher FC between the parietal and frontal lobes (uncorrected $P = 0.005$), as well as between the occipital and parietal lobes (uncorrected $P = 0.019$) (Fig. 6G). At the regional level, we analyzed 101 predefined brain regions, which included 88 cortical and 13 subcortical regions per hemisphere. Consistent with prior findings, 18 regions showed higher functional connectivity density (FCD), predominantly in the parietal lobe ($n = 8$, Fig. 6I and J), including fundus intraparietal sulcus (uncorrected $P < 0.001$), area 23 (uncorrected $P = 0.005$), area 30 (uncorrected $P = 0.006$), area 7op (uncorrected $P = 0.008$), medial intraparietal area (uncorrected $P = 0.025$), anterior intraparietal area (uncorrected $P = 0.032$), V6 (uncorrected $P = 0.040$), and lateral intraparietal area (uncorrected $P = 0.044$). Additionally, significant increases in FCD were observed in 3 frontal lobe regions (area 24c prime, uncorrected $P = 0.011$; area 44, uncorrected $P = 0.036$; and area 24a/b prime, uncorrected $P = 0.018$) and one occipital lobe region (middle temporal area, uncorrected $P = 0.040$) (Fig. 6I and J).

The temporal lobe analysis revealed significant changes in FCD across 6 regions; however, only one region (caudomedial belt region, uncorrected $P = 0.031$) showed increased FCD, while 5 regions demonstrated decreased FCD (area 35, uncorrected $P = 0.007$; rostral areas of the core, uncorrected $P = 0.016$; rostral ERh, uncorrected $P = 0.038$; rostral areas of the lateral belt, uncorrected $P = 0.039$; and agranular temporal pole, uncorrected $P = 0.044$) in self-injury macaques (Fig. 6I and J). NBS identified differing FC between region pairs in self-injury macaques and those in controls. As the primary threshold increased, a stable set of differing functional connections persisted, with results at a high threshold ($t = 4$) shown in Fig. S2D. Notably, most of the increased FC in self-injury macaques was localized between the frontal and parietal lobes ($n = 55$) (Fig. S2E), while only 7 connections showed reduced strength in self-injury macaques compared with those in controls (Fig. S2F).

Ketamine treatment had no therapeutic effect on SIB

Ketamine, as an *N*-methyl-D-aspartate receptor antagonist, has been revealed to have robust antidepressant effects and probably antisuicidal effects through impact on glutamate neurotransmission [18,19] and the FC of the subgenual anterior cingulate cortex [20]. We tested the potential treatment effect of ketamine (1.0 mg/kg, 3.5 weeks, 2 injections per week) in self-injury macaques and found no difference in wound score and behavior characteristics between prior ketamine and post-ketamine administration. Similarly, no change was found in macaques' body weight, blood cortisol, 5-HT, and oxytocin. Therefore, a low dose of ketamine had no treatment effect on macaques with SIB.

Discussion

Spontaneously, self-injury macaques may exhibit a potential translational value as a model for NSSI in humans, demonstrating overlapping behavioral, neurobiological, and neuroimaging features. When a battery of behavioral paradigms was conducted, the self-injury macaques exhibited similar outcomes to human NSSI, reflected by reduced locomotor activity [9] and social interaction, impaired sensory function characterized by hypoalgesia [11], emotional dysregulation [21,22], and deficient cognition and flexibility [23,24] when compared with the controls. Neurochemical analyses revealed diminished

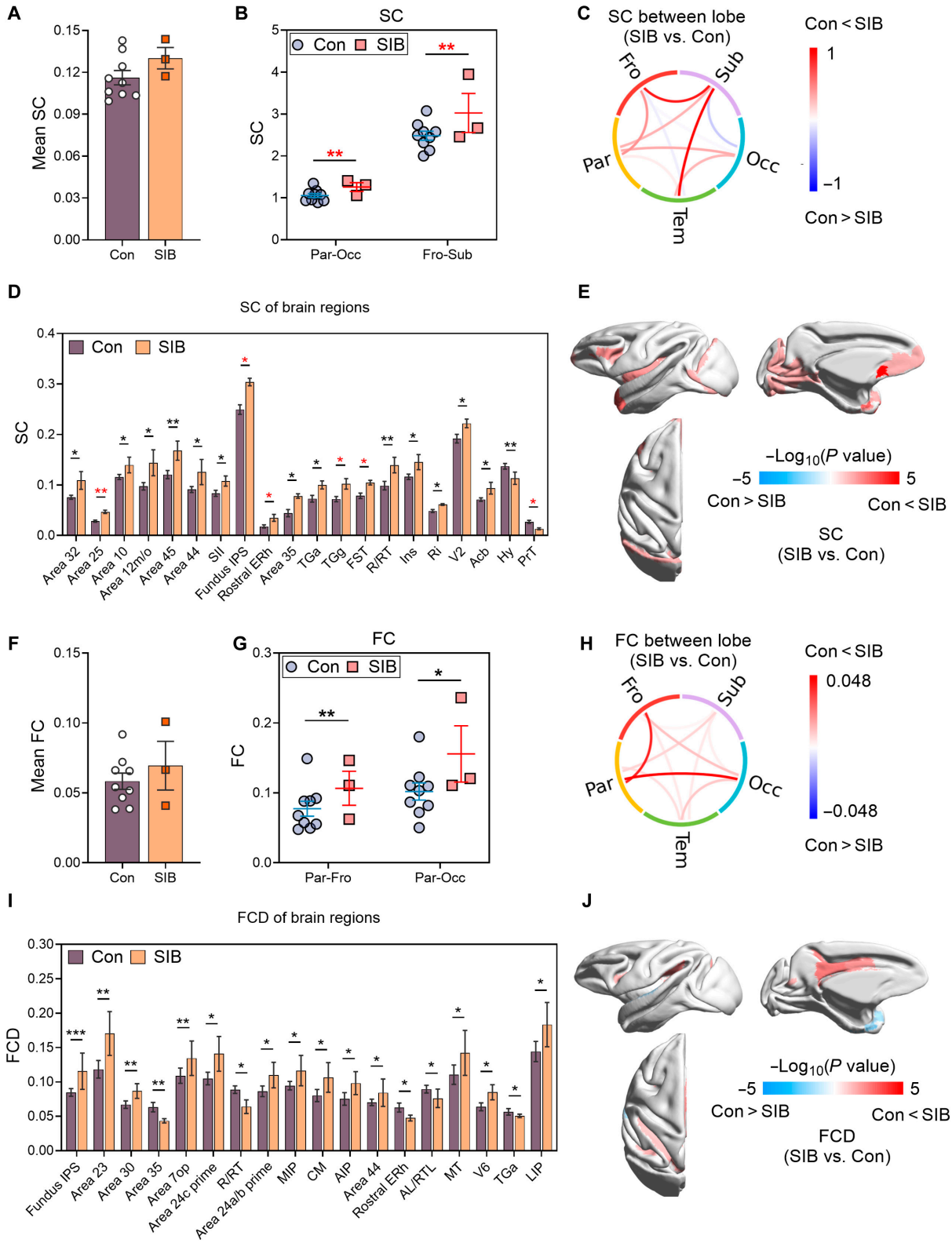

Fig. 6. Differences in structural connectivity (SC) and functional connectivity (FC) between macaques with SIB and controls. (A) Mean SC at the whole-brain level in self-injury macaques (SIB) versus controls (Con). (B) Bar plot showing significant differences in SC between lobes in self-injury macaques and those in controls. (C) Comparison of average SC between lobes for the 2 groups. (D) Bar plots showing SC for regions with significant differences between SIB and Con. (E) Visualization of brain regions with significant differences on the mid-gray surfaces of the macaque template. Red indicates regions where SC is greater in self-injury macaques, while blue indicates the opposite. (F) Mean FC at the whole-brain level in SIB versus Con. (G) Whisker plot showing significant differences in FC between lobes in SIB and those in Con. (H) Comparison of average FC between lobes for the 2 groups. (I) Bar plots showing functional connectivity density (FCD) for regions with significant differences between SIB and Con. (J) Visualization of brain regions with significant differences on the mid-gray surfaces of the macaque template. Red indicates regions where FCD is greater in self-injury macaques than in controls, while blue indicates the opposite. The abbreviations and the names of the brain regions are shown in Table S4. SIB, $n = 3$; Con, $n = 9$.

serotonergic activity, abnormal cortisol, and reduced oxytocin levels, potentially underlying emotional deficits. Structural neuroimaging showed amygdala enlargement (linked to human suicidality [25]) and reduced GMV in frontal regions (e.g., PFC and OFC), aligning with human findings of emotional dysregulation, stress hypersensitivity, and behavioral disinhibition.

Importantly, the self-injury macaques demonstrated impaired performance in the SWM and RL tasks, which have been proven to be the responsibility of the PFC [26]. A significantly high bias score, low win–stay, and high win–shift were found in self-injury macaques, suggesting that compulsivity and impulsivity might be an implicit cause of SIB, as observed in NSSI [15]. Impaired response inhibition—a core component of impulsivity—was also reflected by a shorter reaction time while making decision in self-injury macaques. Dysfunctional PFC activity was consistent with our neuroimaging results that significant reductions in the GMV including large areas of the PFC, including area 45, area 46d, and area 46v/f, were found in self-injury macaques.

HPA axis dysregulation in NSSI patients, particularly those with comorbid depression, may drive SIB via cortisol deficiency impairing cognition and impulse control [27,28]. Reduced 5-HT, critical for mood regulation, is observed in psychiatric patients and self-injury macaques [17]. Aligning with the deficit in paired social interaction, oxytocin, a neuropeptide modulating social bonding, had a tendency to have a lower level in the CSF of self-injury macaques. Oxytocin has been understudied in NSSI, although low CSF oxytocin correlates with suicidal intent [16,29]. A hypothesis posits that impaired self-perception in NSSI patients triggers social dysfunction, prompting self-injury to seek connection [24]. This study first reported lower plasma oxytocin, alongside significantly reduced cortisol and 5-HT in self-injury macaques, validating NHP models for clinical biomarker exploration in NSSI. These findings highlight intertwined neuroendocrine dysfunctions in NSSI pathology.

Metabolomic analysis may address the research gap in biomarkers for NSSI. Adolescents with NSSI exhibit reduced gut microbiota diversity [30], which correlates with the abnormal activation of digestive pathways in self-injury macaques. Dopamine is implicated in NSSI-related psychiatric mechanisms [31]. Additionally, inositol metabolite abnormalities linked to mood disorders [32] align with the observed down-regulation of phosphatidylinositol signaling in these macaques. Their distinct metabolic profiles, differing markedly from controls, mirror findings in NSSI animal models and bipolar disorder patients [17,33]. These findings suggest that metabolomic dysregulation and neural signaling disruptions may jointly underlie NSSI pathogenesis. Further confirmation should involve comparison with the human metabolome to identify the biomarkers, so as to predict disease.

In addition, we found that one male self-injury macaque showed extremely high inflammatory factors (neutrophil-to-lymphocyte ratio, monocyte-to-lymphocyte ratio, and platelet-to-lymphocyte ratio) (data not shown), which are inflammatory biomarkers linked to human suicidal behavior [34]. Another male exhibited a high testosterone/cortisol ratio (data not shown), correlating with impulsivity in male suicide attempters [35], suggesting inflammatory and neuroendocrine mechanisms in SIB. Enlarging the sample size may reduce the individual difference and highlight the biomarkers associated with SIB.

Although NSSI behaviors and biomarkers show high similarity between humans and NHPs [6], few studies have examined neuroimaging changes in self-injury macaques. Our study revealed significant brain morphometric alterations in these macaques, including subcortical structural changes, enlarged ventricles, and reduced GMV, particularly in the frontal lobe, consistent with human NSSI findings. Previous human studies associate suicidal behavior with volume changes in subcortical regions including the caudate [36], putamen [37], thalamus [38], amygdala [25], and hippocampus [39], while ventricular enlargement is linked to psychiatric disorders with high suicide risk [40]. GMV reductions in PFC, anterior cingulate cortex, and insula are also tied to self-injurious thoughts [41], which here may contribute to emotional dysregulation in macaques. Additionally, self-injury macaques exhibited enhanced SC and FC. SC increases were concentrated between parietal-occipital lobes and frontal-subcortical regions, with NBS highlighting frontal–temporal–subcortical connections—aligning with WM abnormalities in human suicidal behavior [42]. FC enhancements spanned the whole brain, notably between parietal–frontal and occipital–parietal lobes. NBS localized heightened FC to frontal–parietal networks, potentially linked to impaired executive control. Human NSSI studies describe varied fMRI patterns: moderate NSSI correlates with elevated amygdala activation to threats, while severe NSSI shows reduced amygdala–medial PFC connectivity [43]. Although animal rs-fMRI is limited by anesthesia, the widespread connectivity changes in macaques may explain multimodal neuroimaging abnormalities and guide therapeutic targets; for example, reduction of the SC and FC between the cortico-limbic network responsible for emotional response may need to be tested in macaques. The limited SC–FC overlap reflects their differing biological bases: SC represents direct anatomical pathways, whereas FC captures dynamic, multisynaptic interactions [44,45]. These neuroimaging findings align with behavioral parallels. NSSI-related impulsivity in adolescents is theorized to stem from limbic-PFC developmental imbalance [46], with structural and functional deficits in these regions contributing to self-harm [47]. Our observations of concurrent behavioral and MRI abnormalities in macaques further support their validity as models for human NSSI, offering insights into neurobiological mechanisms and potential interventions. Future investigations should extend the circuit level by activation and inhibition of certain brain regions combined with optogenetic and chemogenomic techniques and also explore physical interventions.

Our study assessed low-dose ketamine's effect on SIB in macaques but observed no reduction in SIB severity or hormonal changes. Potential reasons may include the following: Firstly, ketamine's rapid antidepressant/antisuicidal efficacy [18,19] may not apply here, as SIB macaques lacked overt depressive symptoms (e.g., withdrawal and low interest). Secondly, ketamine's analgesic properties [48] might paradoxically sustain SIB in macaques with preexisting pain sensitivity dysfunction. Thirdly, intramuscular administration (vs. intravenous) could limit efficacy. Future investigations should increase macaque sample size and systematically evaluate pharmacological interventions and reveal dose-depending characteristics through comparative analysis of intravenous versus intramuscular administration routes. Notably, selecting self-injury macaques with depressive phenotypes, which hospitals often report, could enhance the efficiency and precision of translational research by establishing clinically relevant pharmacological profiles.

We cannot avoid the interspecies limitation on modeling human diseases; that is, NSSI cannot be fully manifested in animals, and basically, it is difficult to detect suicidal intent in animals for suicidal acts involves will, planning, and intention. However, just like most other human mental disorders, when

we focus on every single step leading to the disorders, we can use animal models to mirror the specific aspects or traits of human diseases and assess the pathogenesis and intervention [49]. Here, the endophenotypes, e.g., neurobiological, endocrine, neuroanatomical, cognitive, and emotional measures, associated with NSSI behavior could be translatable to animal models, particularly spontaneously self-injury macaques, and may support insight into therapeutic strategies.

On the other hand, SIB, due to the pattern of repetitive stereotypies, is involved in neurodevelopmental disorders, e.g., 40% to 50% of autism spectrum disorder. In autistic youth, emotional dysregulation, higher hypersensitivity, lower intelligence quotient, and poor speech level were associated with greater severity of SIB topographies depending on different subtypes [50]. In the current experiment, we found that 2 self-injury macaques showed lower social interaction, which was consistent with autism spectrum disorder [1], also common in NSSI individuals, while approaching behavior failed to show a difference, probably because the size of the testing cage was limited.

Moreover, SIB may also be diagnosed as stereotypic movement disorder according to DSM-5 [1]. We found that self-injury macaques showed unique repetitive SIB (half leg-biting, another half arm-biting). Considering that stereotypic movement disorder is diagnosed as broader stereotypes, we recommend this macaque model to be used for studying the specific components of NSSI and developing an intervention. With artificial-intelligence-assisted precise analysis, limiting anthropomorphization by behavioral quantitative aspects may be helpful to translate behavioral research from human to animal studies.

On the other hand, SIB can be studied independently of diagnoses; for example, the Research Domain Criteria Project suggested that NSSI is likely to be clarified not by applying psychiatric diagnoses but by understanding the diverse underlying biological mechanisms that lead to this behavior. They encouraged that NSSI studies should examine neurobiological constructs (negative valence, positive valence, cognitive and social processes, and arousal/regulatory systems) across multiple units of analysis and assess how systems change across the development and course of illness [4]. It is particularly suitable for studies on animal models because animals cannot fully mimic NSSI-involved human diseases.

Other limitations include the following: The SIB biological rhythm was under a slight stress from transferring macaques into a novel environment, and the observation was over only 3 consecutive days; therefore, the stability of the biological pattern is uncertain. Future study may need to address SIB biological rhythm pattern under a naturalistic conditions including nighttime monitoring for extending the observation period and a longitudinal study across different seasons. Furthermore, we cannot avoid the intraspecies limitation due to a small sample size, leading to endophenotypical interpretation challenges. It is worthy studying the correlation between SIB severity and neuroendocrine, neuroanatomical, sensitivity, cognitive, and emotional measures and social interaction across the aspects of age and gender in large samples, providing insight into key predictors of SIB subtopography. In addition, considering that most SIB was found in the single-housed macaques, aligned with Nock and Prinstein's dual-dimension model [51] categorizing intrapersonal (e.g., emotion regulation) and interpersonal (e.g., social) functions through negative/positive reinforcement, these macaques engage in cyclical self-injury for sensory stimulation in deprived environments. Environmental stressors or social isolation may exacerbate SIB severity. This mirrors human NSSI mechanisms where behavioral patterns serve as maladaptive coping strategies. In the future, we also need to evaluate whether these animals may reduce SIB when they are group-housed, or oppositely, the social stress may increase their SIB, to identify the environmental effects.

Finally, we propose that future research incorporate expanded macaque cohorts to cross-species integrate mechanistic data from NHP studies with human clinical data, emphasizing critical applications: (a) phenotypic refinement by dissecting subtype-specific characteristics/traits aligning with NSSI individuals and revealing the sequence of the physiological and behavioral patterns pre- and post-self-injury; (b) circuit-level analysis by utilizing advanced neuroimaging, optogenetic, and chemogenomic techniques in NHPs to map brain networks disrupted in SIB for application in precise diagnosis and prediction of the therapies; (c) physiological research and screen biomarkers by making comparison between human and animals in the central nervous and periphery systems, particular neuroendocrine and inflammatory factors, to enhance understanding of the etiology of diseases and advance targeted interventions; and (d) therapeutic research and translation by longitudinally studying various pharmacological and physical interventions on the macaque model of SIB. Pharmacological interventions involve antidepressants, atypical antipsychotics, opioid antagonists, etc. Physical interventions involve transcranial magnetic stimulation, transcranial direct/alternating current stimulation, and deep brain stimulation (DBS) As for those that have been already adopted in clinical treatments, more focused experimental research studies are required to elucidate their underlying mechanisms, especially when it comes to NHPs. Meanwhile, NHP models could be used to evaluate the effectiveness of new techniques for intervention, which cannot be conducted in humans.

Altogether, the self-injury macaque model's ecological validity supports its utility of underlying NSSI pathogenesis of specific components, offering insights for translational research on SIB across species. Mechanistic research on NHPs remains critical to bridge gaps between preclinical and therapeutic outcomes. This highlights the need for tailored approaches when translating interventions into complex behavioral disorders like SIB, particularly in NHPs with distinct neurobiological profiles.

Materials and Methods

For details about the materials and methods, please see the Supplementary Materials.

Acknowledgments

We thank Prof. Peng-Fei Wei and Mr. Guo-Ling Tang for assisting in the analysis of the macaque 3D social interaction test and Dr. Nan-Hui Chen, Mr. Wei-Jie Jin, and the Core Technology Facility, KIZ, CAS, for providing MRI services. We thank the staff of the National Research Facility for Phenotypic & Genetic Analysis of Model Animals (Primate Facility) (https://cstr.cn/31137.02.NPRC) for providing technical support and assistance in data collection and analysis.

Funding: This work was supported by STI2030-Major Projects (2022ZD0205100 to J.-H.W., 2021ZD0203900 to J.-H.W., 2021-ZD0200900 to Y.-G.Y., 2021ZD0200200 to N.L., and 2021-ZD0204200 to Y.-C.Q.), Yunnan Province (202305AH340006 to Y.-G.Y.), the "Light of West China" Program of the Chinese

Academy of Sciences (xbzg-zdsys-202302 to Y.-G.Y.), and the High Level Hospital Construction Project of Jiangsu Province to C.W.

Author contributions: Y.-L.Z., H.-D.H., Y.-F.Z., Y.-L.L., H.-M.Z., S.-Z.D., and M.-H.Q. performed behavioral, physical, and MRI experiments. Y.-C.Q., J.-X.R., and S.-S.Y. performed MRI analysis and writing. Y.-C.J., C.-Y.L., H.-H.X., C.-K.Y., K.H., and H.-L.C. conducted ketamine treatment and 3D experiments. L.Z., B.-L.Z., and S.L. contributed to metabolism analysis and writing. Q.Z., S.-C.W., X.-M.Y., Y.W., Q.W., Y.-J.L., Y.X., and L.-B.L. collected physiological data. Y.-G.Y., N.L., and C.W. supported the experiments and revised the manuscript. J.-H.W. wrote the manuscript and supported and supervised the experiments.

Competing interests: The authors declare that they have no competing interests.

Data Availability

The data are freely available upon request.

Supplementary Materials

Materials and Methods
Tables S1 to S4
Figs. S1 and S2
Movies S1 and S2
References [52–79]

References

1. American Psychiatric Association. *Diagnostic and statistical manual of mental disorders*, 5th edition ed.Washington (DC): American Psychiatric Association; 2013.
2. Zhang P, Ouyang L, Liang M, Wu Y, Bao C, Yang K, Liu Y, Long J, Wang X, Liu G, et al. A cross-sectional epidemiological study of non-suicidal self-injury prevalence in Chinese psychiatric patients. *Nat. Mental Health*. 2023;1(4):266–272.
3. Yan WJ, Huang HY, Ruan QN, Wu YW, Xu S, Zhao K. The functional heterogeneity of non-suicidal self-injury: Insights from latent profile analysis. *BMC Psychiatry*. 2024;24(1):948.
4. Westlund Schreiner M, Klimes-Dougan B, Begnel ED, Cullen KR. Conceptualizing the neurobiology of non-suicidal self-injury from the perspective of the Research Domain Criteria Project. *Neurosci Biobehav Rev*. 2015;57:381–391.
5. Lawrence HR, Balkind EG, Ji JL, Burke TA, Liu RT. Mental imagery of suicide and non-suicidal self-injury: A meta-analysis and systematic review. *Clin Psychol Rev*. 2023;103:Article 102302.
6. Novak MA, Meyer JS. A rhesus monkey model of non-suicidal self-injury. *Front Behav Neurosci*. 2021;15:Article 674127.
7. Campos AI, Verweij KJH, Statham DJ, Madden PAF, Maciejewski DF, Davis KAS, John A, Hotopf M, Heath AC, Martin NG, et al. Genetic aetiology of self-harm ideation and behaviour. *Sci Rep*. 2020;10(1):9713.
8. Yuan X, Devine DP. The role of anxiety in vulnerability for self-injurious behaviour: Studies in a rodent model. *Behav Brain Res*. 2016;311:201–209.
9. Boone SD, Brausch AM. Physical activity, exercise motivations, depression, and nonsuicidal self-injury in youth. *Suicide Life Threat Behav*. 2016;46(5):625–633.
10. Huang W, Zong J, Zhang Y, Zhou Y, Zhang L, Wang Y, Shan Z, Xie Q, Li M, Pan S, et al. The role of circadian rhythm in neurological diseases: A translational perspective. *Aging Dis*. 2024;15(4):1565–1587.
11. Kao HT, Murner-Lavanchy I, von Stosch E, Josi J, Berger T, Koenig J, Kaess M. Pain sensitivity as a state marker and predictor for adolescent non-suicidal self-injury. *Psychol Med*. 2024;54(9):2291–2298.
12. Nilsson M, Lundh L, Westrin A, Westling S. Executive functioning in psychiatric patients with deliberate self-harm, as compared with a psychiatric and a healthy comparison group. *J Clin Exp Neuropsychol*. 2021;43(3):225–237.
13. Freeman ZT, Rice KA, Soto PL, Pate KA, Weed MR, Ator NA, DeLeon IG, Wong DF, Zhou Y, Mankowski JL, et al. Neurocognitive dysfunction and pharmacological intervention using guanfacine in a rhesus macaque model of self-injurious behavior. *Transl Psychiatry*. 2015;5(5):Article e567.
14. Ota K, Charles L, Haggard P. Autonomous behaviour and the limits of human volition. *Cognition*. 2024;244:Article 105684.
15. Lutz NM, Chamberlain SR, Goodyer IM, Bhardwaj A, Sahakian BJ, Jones PB, Wilkinson PO. Behavioral measures of impulsivity and compulsivity in adolescents with nonsuicidal self-injury. *CNS Spectr*. 2022;27(5):604–612.
16. Jahangard L, Shayganfard M, Ghiasi F, Salehi I, Haghighi M, Ahmadpanah M, Sadeghi Bahmani D, Brand S. Serum oxytocin concentrations in current and recent suicide survivors are lower than in healthy controls. *J Psychiatr Res*. 2020;128:75–82.
17. Cohen RL, Drewes JL, Queen SE, Freeman ZT, Pate KM, Adams RJ, Graham DR, Hutchinson EK. Elucidation of the central serotonin metabolism pathway in rhesus macaques (*Macaca mulatta*) with self-injurious behavior. *Comp Med*. 2021;71(6):466–473.
18. Autry AE, Adachi M, Nosyreva E, Na ES, Los MF, Cheng P-f, Kavalali ET, Monteggia LM. NMDA receptor blockade at rest triggers rapid behavioural antidepressant responses. *Nature*. 2011;475(7354):91–95.
19. Kritzer MD, Mischel NA, Young JR, Lai CS, Masand PS, Szabo ST, Mathew SJ. Ketamine for treatment of mood disorders and suicidality: A narrative review of recent progress. *Ann Clin Psychiatry*. 2021;34(1):33–43.
20. Hashimoto K. Rapid-acting antidepressant ketamine, its metabolites and other candidates: A historical overview and future perspective. *Psychiatry Clin Neurosci*. 2019.
21. Calvete E, Royuela-Colomer E, Maruottolo C. Emotion dysregulation and mindfulness in non-suicidal self-injury. *Psychiatry Res*. 2022;314:Article 114691.
22. Guerin-Marion C, Bureau JF, Lafontaine MF, Gaudreau P, Martin J. Profiles of emotion dysregulation among university students who self-injure: Associations with parent–child relationships and non-suicidal self-injury characteristics. *J Youth Adolesc*. 2021;50(4):767–787.
23. Wu DD, Zhang BL, Chen Y, Zhang Y, Qiao Y, Wu Y, Zhang Y, Lu Y, You X, Li Y, et al. Forward and reverse genomic screens enhance the understanding of phenotypic variation in a large Chinese rhesus macaque cohort. Research Square. 2024. https://doi.org/10.21203/rs.3.rs-4800799/v1
24. Sorgi-Wilson KM, Cheung JC, Ciesinski NK, McCloskey MS. Cognition and non-suicidal self-injury: Exploring relationships with psychological functions. *Arch Suicide Res*. 2022;27(3):1002–1018.
25. Monkul ES, Hatch JP, Nicoletti MA, Spence S, Brambilla P, Lacerda ALT, Sassi RB, Mallinger AG, Keshavan MS, Soares JC. Fronto-limbic brain structures in suicidal and non-suicidal

female patients with major depressive disorder. *Mol Psychiatry*. 2007;12(4):360–366.
26. Diamond A. Executive functions. *Annu Rev Psychol*. 2013;64(1):135–168.
27. Klimes-Dougan B, Begnel E, Almy B, Thai M, Schreiner MW, Cullen KR. Hypothalamic-pituitary-adrenal axis dysregulation in depressed adolescents with non-suicidal self-injury. *Psychoneuroendocrinology*. 2019;102:216–224.
28. Peng B, Wang R, Zuo W, Liu H, Deng C, Jing X, Hu H, Zhao W, Qin P, Dai L, et al. Distinct correlation network of clinical characteristics in suicide attempters having adolescent major depressive disorder with non-suicidal self-injury. *Transl Psychiatry*. 2024;14(1):134.
29. Jokinen J, Chatzittofis A, Hellström C, Nordström P, Uvnäs-Moberg K, Åsberg M. Low CSF oxytocin reflects high intent in suicide attempters. *Psychoneuroendocrinology*. 2012;37(4):482–490.
30. Cai LF, Wang SB, Hou CL, Li ZB, Liao YJ, Jia FJ. Association between non-suicidal self-injury and gut microbial characteristics in Chinese adolescent. *Neuropsychiatr Dis Treat*. 2022;18:1315–1328.
31. Turner BJ, Austin SB, Chapman AL. Treating nonsuicidal self-injury: A systematic review of psychological and pharmacological interventions. *Can J Psychiatr*. 2014;59(11):576–585.
32. Concerto C, Chiarenza C, Di Francesco A, Natale A, Privitera I, Rodolico A, Trovato A, Aguglia A, Fisicaro F, Pennisi M, et al. Neurobiology and applications of inositol in psychiatry: A narrative review. *Curr Issues Mol Biol*. 2023;45(2):1762–1778.
33. Guo X, Jia J, Zhang Z, Miao Y, Wu P, Bai Y, Ren Y. Metabolomic biomarkers related to non-suicidal self-injury in patients with bipolar disorder. *BMC Psychiatry*. 2022;22(1):491.
34. Amitai M, Kaffman S, Kroizer E, Lebow M, Magen I, Benaroya-Milshtein N, Fennig S, Weizman A, Apter A, Chen A. Neutrophil to-lymphocyte and platelet-to-lymphocyte ratios as biomarkers for suicidal behavior in children and adolescents with depression or anxiety treated with selective serotonin reuptake inhibitors. *Brain Behav Immun*. 2022;104:31–38.
35. Stefansson J, Chatzittofis A, Nordstrom P, Arver S, Asberg M, Jokinen J. CSF and plasma testosterone in attempted suicide. *Psychoneuroendocrinology*. 2016;74:1–6.
36. Wagner G, Koch K, Schachtzabel C, Schultz CC, Sauer H, Schlosser RG. Structural brain alterations in patients with major depressive disorder and high risk for suicide: Evidence for a distinct neurobiological entity? *NeuroImage*. 2011;54(2):1607–1614.
37. Ho TC, Cichocki AC, Gifuni AJ, Catalina Camacho M, Ordaz SJ, Singh MK, Gotlib IH. Reduced dorsal striatal gray matter volume predicts implicit suicidal ideation in adolescents. *Soc Cogn Affect Neurosci*. 2018;13(11):1215–1224.
38. Lopez-Larson M, King JB, McGlade E, Bueler E, Stoeckel A, Epstein DJ, Yurgelun-Todd D. Enlarged thalamic volumes and increased fractional anisotropy in the thalamic radiations in veterans with suicide behaviors. *Front Psych*. 2013;4:83.
39. Colle R, Chupin M, Cury C, Vandendrie C, Gressier F, Hardy P, Falissard B, Colliot O, Ducreux D, Corruble E. Depressed suicide attempters have smaller hippocampus than depressed patients without suicide attempts. *J Psychiatr Res*. 2015;61:13–18.
40. Johnston JAY, Wang F, Liu J, Blond BN, Wallace A, Liu J, Spencer L, Cox Lippard ET, Purves KL, Landeros-Weisenberger A, et al. Multimodal neuroimaging of frontolimbic structure and function associated with suicide attempts in adolescents and young adults with bipolar disorder. *Am J Psychiatry*. 2017;174(7):667–675.
41. Schmaal L, van Harmelen AL, Chatzi V, Lippard ETC, Toenders YJ, Averill LA, Mazure CM, Blumberg HP. Imaging suicidal thoughts and behaviors: A comprehensive review of 2 decades of neuroimaging studies. *Mol Psychiatry*. 2020;25(2):408–427.
42. Yurgelun-Todd DA, Bueler CE, McGlade EC, Churchwell JC, Brenner LA, Lopez-Larson MP. Neuroimaging correlates of traumatic brain injury and suicidal behavior. *J Head Trauma Rehabil*. 2011;26(4):276–289.
43. Başgöze Z, Mirza SA, Silamongkol T, Hill D, Falke C, Thai M, Westlund Schreiner M, Parenteau AM, Roediger DJ, Hendrickson TJ, et al. Multimodal assessment of sustained threat in adolescents with nonsuicidal self-injury. *Dev Psychopathol*. 2021;33(5):1774–1792.
44. Suarez LE, Markello RD, Betzel RF, Misic B. Linking structure and function in macroscale brain networks. *Trends Cogn Sci*. 2020;24(4):302–315.
45. Damoiseaux JS, Greicius MD. Greater than the sum of its parts: A review of studies combining structural connectivity and resting-state functional connectivity. *Brain Struct Funct*. 2009;213(6):525–533.
46. Mills KL, Goddings AL, Clasen LS, Giedd JN, Blakemore SJ. The developmental mismatch in structural brain maturation during adolescence. *Dev Neurosci*. 2014;36(3–4):147–160.
47. Auerbach RP, Pagliaccio D, Allison GO, Alqueza KL, Alonso MF. Neural correlates associated with suicide and nonsuicidal self-injury in youth. *Biol Psychiatry*. 2021;89(2):119–133.
48. Riccardi A, Guarino M, Serra S, Spampinato M, Vanni S, Shiffer D, Voza A, Fabbri A, De Iaco F. Narrative review: Low-dose ketamine for pain management. *J Clin Med*. 2023;12(9):3256.
49. Preti A. Animal model and neurobiology of suicide. *Prog Neuro-Psychopharmacol Biol Psychiatry*. 2011;35(4):818–830.
50. Ferguson EF, Spackman E, Cai RY, Hardan AY, Uljarevic M. Exploring the heterogeneity of self-injurious behaviors in autistic youth: Patterns, predictors, and implications for intervention. *Autism Res*. 2025;18(1):133–151.
51. Nock MK, Prinstein MJ. A functional approach to the assessment of self-mutilative behavior. *J Consult Clin Psychol*. 2004;72(5):885–890.
52. Freeman ZT, Krall C, Rice KA, Adams RJ, Metcalf Pate KA, Hutchinson EK. Severity and distribution of wounds in rhesus macaques (*Macaca mulatta*) correlate with observed self-injurious behavior. *J Am Assoc Lab Anim Sci*. 2015;54(5):516–520.
53. Huang K, Han Y, Chen K, Pan H, Zhao G, Yi W, Li X, Liu S, Wei P, Wang L. A hierarchical 3D-motion learning framework for animal spontaneous behavior mapping. *Nat Commun*. 2021;12(1):2784.
54. Tang G, Han Y, Sun X, Zhang R, Han MH, Liu Q, Wei P. Anti-drift pose tracker (ADPT), a transformer-based network for robust animal pose estimation cross-species. *eLife*. 2025;13:Article RP95709.
55. Kezar SM, Baker KC, Russell-Lodrigue KE, Bohm RP. Single-dose diazepam administration improves pairing success of unfamiliar adult male rhesus macaques (*Macaca mulatta*). *J Am Assoc Lab Anim Sci*. 2022;61(2):173–180.

56. Yang L, Han B, Zhang Z, Wang S, Bai Y, Zhang Y, Tang Y, Du L, Xu L, Wu F, et al. Extracellular vesicle-mediated delivery of circular RNA SCMH1 promotes functional recovery in rodent and nonhuman primate ischemic stroke models. *Circulation*. 2020;142(6):556–574.
57. Pujara MS, Rudebeck PH, Ciesinski NK, Murray EA. Heightened defensive responses following subtotal lesions of macaque orbitofrontal cortex. *J Neurosci*. 2019;39(21): 4133–4141.
58. Kalin NH, Shelton SE. Defensive behaviors in infant rhesus monkeys: Environmental cues and neurochemical regulation. *Science*. 1989;243(4899):1718–1721.
59. Coleman K, Robertson ND, Dissen GA, Neuringer MD, Martin LD, Cuzon Carlson VC, Kroenke C, Fair D, Brambrink AM. Isoflurane anesthesia has long-term consequences on motor and behavioral development in infant rhesus macaques. *Anesthesiology*. 2017;126(1):74–84.
60. Bliss-Moreau E, Santistevan AC, Bennett J, Moadab G, Amaral DG. Anterior cingulate cortex ablation disrupts affective vigor and vigilance. *J Neurosci*. 2021;41(38): 8075–8087.
61. Huang HD, Pu JL, Zhou YF, Fan Y, Zhang YL, Li YL, Chen YZ, Wang Y, Yu XM, Dmitry B, et al. A spontaneous hyperglycaemic cynomolgus monkey presents cognitive deficits, neurological dysfunction and cataract. *Clin Exp Pharmacol Physiol*. 2024;51(6):Article e13863.
62. Halloran MA, Zentall TR. The midsession reversal task with pigeons does a brief delay between choice and reinforcement facilitate reversal learning? *Behav Process*. 2020;177: Article 104150.
63. Vincent JL, Patel GH, Fox MD, Snyder AZ, Baker JT, Van Essen DC, Zempel JM, Snyder LH, Corbetta M, Raichle ME. Intrinsic functional architecture in the anaesthetized monkey brain. *Nature*. 2007;447(7140):83–86.
64. Larson-Prior LJ, Zempel JM, Nolan TS, Prior FW, Snyder AZ, Raichle ME. Cortical network functional connectivity in the descent to sleep. *Proc Natl Acad Sci USA*. 2009;106(11): 4489–4494.
65. Cox RW. AFNI: Software for analysis and visualization of functional magnetic resonance neuroimages. *Comput Biomed Res*. 1996;29(3):162–173.
66. Jenkinson M, Beckmann CF, Behrens TE, Woolrich MW, Smith SM. FSL. *NeuroImage*. 2012;62(2):782–790.
67. Avants BB, Tustison N, Johnson H. Advanced Normalization Tools (ANTS): V1.0. *Insight J*. 2014;1–35.
68. Fischl B. FreeSurfer. *NeuroImage*. 2012;62(2):774–781.
69. Jung B, Taylor PA, Seidlitz J, Sponheim C, Perkins P, Ungerleider LG, Glen D, Messinger A. A comprehensive macaque fMRI pipeline and hierarchical atlas. *NeuroImage*. 2021;235:Article 117997.
70. Hartig R, Glen D, Jung B, Logothetis NK, Paxinos G, Garza-Villarreal EA, Messinger A, Evrard HC. The Subcortical Atlas of the Rhesus Macaque (SARM) for neuroimaging. *NeuroImage*. 2021;235:Article 117996.
71. Tournier JD, Calamante F, Connelly A. Robust determination of the fibre orientation distribution in diffusion MRI: Non-negativity constrained super-resolved spherical deconvolution. *NeuroImage*. 2007;35(4):1459–1472.
72. Tournier JD. Diffusion MRI in the brain—Theory and concepts. *Prog Nucl Magn Reson Spectrosc*. 2019;112–113:1–16.
73. Smith RE, Tournier JD, Calamante F, Connelly A. SIFT2: Enabling dense quantitative assessment of brain white matter connectivity using streamlines tractography. *NeuroImage*. 2015;119:338–351.
74. Hagmann P, Cammoun L, Gigandet X, Meuli R, Honey CJ, Wedeen VJ, Sporns O. Mapping the structural core of human cerebral cortex. *PLOS Biol*. 2008;6(7):Article e159.
75. Jo HJ, Gotts SJ, Reynolds RC, Bandettini PA, Martin A, Cox RW, Saad ZS. Effective preprocessing procedures virtually eliminate distance-dependent motion artifacts in resting state FMRI. *J Appl Math*. 2013; 10.1155/2013/935154.
76. Weissenbacher A, Kasess C, Gerstl F, Lanzenberger R, Moser E, Windischberger C. Correlations and anticorrelations in resting-state functional connectivity MRI: A quantitative comparison of preprocessing strategies. *NeuroImage*. 2009;47(4):1408–1416.
77. Zalesky A, Fornito A, Bullmore ET. Network-based statistic: Identifying differences in brain networks. *NeuroImage*. 2010;53(4):1197–1207.
78. Xia M, Wang J, He Y. BrainNet viewer: A network visualization tool for human brain connectomics. *PLOS ONE*. 2013;8(7):Article e68910.
79. Nakamura S, Kishimoto Y, Sekino M, Nakamura M, Tsutsui K-I. Depression induced by low-frequency repetitive transcranial magnetic stimulation to ventral medial frontal cortex in monkeys. *Exp Neurol*. 2022;357:Article 114168.

Supplementary Materials for
A study of spontaneous self-injurious behavior and neuroimaging in rhesus macaques

Ya-Li Zhang et al.

Corresponding author: Jian-Hong Wang (wangjh@mail.kiz.ac.cn), Ning Liu (liuning@ibp.ac.cn), Chun Wang (chun_wang@njmu.edu.cn)

The file includes:
Materials and Methods
Table S1 to S4
Figure S1 to S2
Legends for movie S1 to S2

Other Supplementary Material for this manuscript includes the following:
Movie S1
Movie S2

Materials and Methods

Study design

This study aimed to systematically establish behavioral, biochemical, and neuroimaging parallels between spontaneously self-injurious macaques and human non-suicidal self-injury (NSSI) populations, thereby validating this non-human primate (NHP) model for investigating underlying pathogenetic mechanisms and therapeutic interventions. Moreover, considering ketamine has rapid antidepressant effects and probably anti-suicidal properties mediated by glutamatergic modulation [19, 20], we further investigated the effect of low-dose ketamine in this animal model.

Quantitative behavioral assessments in spontaneous SIB macaques were categorized into three domains: General behavioral profiling encompassing sequential behavior patterns, biological rhythm analysis of SIB, three-dimensional (3D) movement tracking locomotor activity and paired social interaction, home-cage activity and sleep evaluation, neurological function assessment, and exploratory behavior quantification; Emotional and defensive response measured through stimulus presentation paradigms and human intruder tests (HIT); Cognitive evaluation using spatial working memory (SWM) tasks, reversal learning (RL) assessments, and win-stay-lose-shift (WSLS) strategy analysis. Biochemical profiling included plasma cortisol, serotonin (5-HT), and oxytocin levels, complemented by CSF metabolomic analysis. Multimodal neuroimaging comprised structural MRI, diffusion-weighted MRI (dMRI), and resting-state functional MRI (rs-fMRI).

Behavioral paradigms and biochemical markers were selected based on NSSI clinical presentations. Additionally, we developed a novel AI-assisted behavioral paradigm tracking system for NHP research and performed comprehensive neuroimaging analyses on self-injury macaques. This systematic integration of cross-species phenotypic data facilitates alignment between macaque biomarkers and human NSSI characteristics, ultimately establishing a translational NHP model for NSSI mechanistic exploration and therapeutic development.

Animals

We observed the sequential behaviors from ten self-injury macaques, and randomly chose three self-injury adult rhesus macaques (*Macaca mulatta*) and three age- and gender-matched control macaques (weighing 7.10±0.81 kg, 8.67±1.20 years old, two males and one female per group) from breeding colonies at the Kunming Institute of Zoology (KIZ) were used in the experiments. The macaques were housed individually under standard conditions (12 h light/dark cycle with light on from 07:00–19:00 h; humidity at 60% and temperature at 21 ± 5°C). Macaques had free access to tap water and were punctually supplied with food three times a day. Experiments were performed between 8:00 and 17:00 h. The macaque's body weight was measured every 2-4 weeks by using a transfer cage.

All experimental procedures involving animals were performed in accordance with the guidelines outlined in the Application Format for Ethical Approval for Research Involving Animals and were approved by the Institutional Animal Care and Use Committee (IACUC-PE-2023-05-001) of Kunming Institute of Zoology, Chinese

Academy of Sciences. All efforts were made to minimize animal suffering and to reduce the number of animals required.

Methods

Characterization of the self-injury macaques

Macaques exhibiting SIB were selected through experimenters' reports and confirmed by immediate repetitive SIB manifestation when observers stood and gazed near cages. These behaviors emerged spontaneously under single-housed conditions without intervention.

We conducted continuous behavioral monitoring of ten individually housed macaques over a 14-day observational period to investigate SIB patterns. For each recorded SIB episode, we performed detailed ethological analysis on 2-minute pre- and post-event intervals, systematically examining both potential trigger and consequential behavioral sequences following SIB manifestation. Further, we randomly chose three self-injury adult rhesus macaques to conduct the experiments.

The macaques underwent physical restraint via cloth limb fixation for wound assessment. Wound severity was scored according to Freeman et al. [52]: 1point =superficial <5mm; 2=superficial >5mm; 3=penetrating dermis <5mm; 4=penetrating dermis >5mm.

Behavioral experiments

Behavioral experiments were recorded by cameras and analyzed by two expert observers or using Observer™ software (Noldus Information Technology B.V., Netherlands). A single-blind procedure was used in the experiment and analyses.

Spontaneous behaviors by 3D motion-capture and behavior decomposition

A multi-view video capture device was used to record animal's spontaneous behaviors. In detail, a macaque cage (100 ×100 ×100 cm) with transparent glass walls was installed in the center of the testing room. To ensure comprehensive coverage, four cameras (Intel RealSense D435) were strategically mounted on supporting pillars, 1.1 meter from the cage, with angles meticulously adjusted to capture a clear and unobstructed view of the entire experimental arena from each camera's perspective. The macaque was gently moved into the behavior testing cage by using a transfer box and its behavior images were simultaneously acquired by four cameras at a frame rate of 30 Hz, with a resolution of 848 × 480 pixels.

The video data collection and analyses were managed by the BehaviorAtlas NHP Explorer and Analyzer software (version 1.01, Shenzhen Bayone BioTech Co.) [53]. A total of 21 key body parts of the macaque were labeled from 4200 frames from eight normal macaques to train a reliable model for identifying experimental macaque's body parts, in which 46 kinematic parameters were extracted and 14 behavioral sequences were constructed based on the parameters. The macaques' behaviors with/without apparent displacement (AD/NAD) were categorized and analyzed individually. Principal component analysis (PCA) was performed on the standardized kinematic parameters, with the cumulative proportion of variance explained by the first principal component (PC1) and the second principal component

(PC2) accounting for 96.00%. The results were standardized using Z-scores. We recorded the spontaneous behaviors of each macaque for 35 min per session, with a total of two sessions with an inter-trial interval (ITI) of a couple of days.

In addition, the self-injury macaque was paired with a gender- and age-matched stranger partner macaque and recorded the social interaction for 35 min per session.

In order to minimize inter-individual difference, each macaque was paired with two strangers × two sessions totally. Each macaque was identified and tracked by using an Anti-drift Pose Tracker (ADPT) [54].

The rump presenting [55], gaze following, approaching behavior, characterized as socially affiliative behaviors, was analyzed according to the following conditions:

Rump presenting behavior: a posture involving a stance on all limbs with the hind quarters elevated and the tail raised, directed at the partner. Gaze following behavior: one macaque looks at the other. Approaching behavior: two macaques sit or stand together, or one macaque approaches to the other with a distance between less than 30 cm within at least 15 consecutive frames (1 second).

In this experiment, two self-injury macaques and three controls were tested, because one male self-injury macaques showing elevated neutrophil-to-lymphocyte ratio (NLR), monocyte-to-lymphocyte ratio (MLR), and platelet-to-lymphocyte ratio (PLR) died.

Home-cage activity and sleep

The ActiGraph GT9X Link (3.5×3.5×1 cm, 14 grams, ActiGraph Corp, USA) was installed on the macaque's collar and used to evaluate the macaque's diurnal activity (timeframe of 7:00–19:00 and nocturnal sleep 19:00-7:00) at the home cage for consecutive eight days (one-day accommodation and middle six-day data analysis). The data were analyzed with the accompanying software ActiLife 6 (ActiGraph Corp., LLC) using a defined time period of 60 sec (epochs). The following activity measures were calculated by two time frames: daily average and maximum VMC (Vector magnitude counts), total activity counts of bouts and sleep (total sleep time, efficiency and sleep fragmentation index).

SIB biological rhythm pattern

Macaques were transferred to a novel observation chamber (100×100×100 cm) for behavioral recording by Kinect 2.0 cameras, during 10:00 - 12:30 a.m. and 14:00 - 16:30 p.m., respectively, over three days. Every middle 30-minute video was analyzed.

Neurological function

Neurological function of macaques was evaluated using a developed neurologic deficit score from our previous study [56], which assigned scores to the motor system (16 points), skeletal muscle coordination (9 points), and the sensory system (25 points), that were tabulated to a total of 50 possible points. Score 0 corresponded to normal behaviors, while higher scores represented neurological deficits. The control animals were 18 adult health macaques.

Exploratory behavior test

We designed an exploratory test in which a neutral fishbone-shaped laser icon (length 11.5 cm, height 4.5 cm) was presented into the macaque's cage by a familiar experimenter positioned 1m front-center, avoiding eye contact. The laser was

executed three 1-min phases: clockwise/counterclockwise cage perimeter movements (5 sec/round) and vertical shaking 5-10 cm near the macaque's abdomen, maintained non-contact to the animal. A Sony HDR-CX405 camera recorded behaviors, with two expert observers scoring via Observer™ software using standardized ethograms. The duration and frequency of macaques' mouth licking, hand touching, and body following with eyes watching were recorded.

Emotional response test

Food preference assessment in macaques was conducted using a Wisconsin General Test Apparatus (WGTA) with a transparent box (55 cm× 20 cm×15 cm). Four food types (hawthorn candy, peanut, raisin, sweet potato) were semi-randomly paired (36 trials/session ×3 sessions), with selections recorded. Subsequently, an emotional response test was conducted modifying from Pujara et al [57]. Novelty response trials (12 trials/session ×3 sessions at two-day intervals) introduced four stimuli (striped rope, plastic tube holder, rubber snake/spider) in the transparent box with favorite food rewards on the top center of the box. Stimuli appeared semi-randomly (2 presentations each) alongside null trials (4/session), maintaining 30-second ITI. The maximum of stimulus presentation was 60 s, with snake toys excluded from initial quadrants and consecutive presentations.

Human intruder test (HIT)

Defensive response to human intruder was tested according to Kalin and Shelton [58], across three sessions over six months. Macaques in relocated cages underwent three sequential 5-minute exposures to unfamiliar intruders: profile orientation with no eye contact (NEC), direct eye contact (EC), and back presentation, each preceded by 3-min acclimation. Intruders maintained 1.0m distance from the cage center during static postures. Affective reactivity to human intruder was scored based on locomotion, stereotypy, defensive position in cage (head in cage's rear half), withdrawal behaviors (freezing, lipsmacking, grimacing, and self-directed biting behaviors), vigilance, aggression (threat, cage shaking behaviors). Particularly, vigilance referred to the duration of the macaque showing attention to and looking at the intruder except of aggressive behavior, while threat referred to the frequency of at least two of the following behaviors directed towards the intruder: intense staring with eyes wide open, lips parted in o shape, head-bob, ear pulled back, bark vocalization or lunges [59, 60].

Spatial working memory (SWM) and Reversal learning (RL)

The SWM was performed by using the WGTA [61]. Six delay lengths (A–F) were semi-randomly assigned per session: A = B×0 s, B = B×1 s, C = B×2 s, D = B×3 s, E = B×4 s, F = B×5 s. Macaques underwent 3-day habituation, followed by B=0 s training until achieving ≥91.67% accuracy (33/36 trials) for 5 consecutive sessions or max 20 sessions. Subsequent B=3 s training lasted 20 sessions. The percentage of correct choice at B=0s/3s and sessions-to-criterion were recorded.

For discrimination learning, macaques distinguished rewarded circles (S+) from non-rewarded diamonds (S−) in 36-trial sessions. After reaching ≥88.89% accuracy (32/36 trials) for 3 sessions (max 20), RL commenced by switching rewards to diamonds. Training continued until the same accuracy criterion or 20-session limit. The percentage of correct choice at each session and sessions-to-criterion were

analyzed. Side preference during RL was calculated as: [(preferred choices−nonpreferred choices)/total choices]×100, reflecting stereotypical behavior.

Win-stay-lose-shift (WSLS)

On the preceding trial of WSLS, reinforcement was provided (win), and the same stimulus should be chosen on the next trial (stay). However, if reinforcement did not occur (lose), on the next trial the other stimulus should be chosen (shift). Usually WSLS was tested in midsession reversal tasks in animals, reflecting the cognitive flexibility, decision-making and impulsivity of animals [62]. Here, WSLS was analyzed with MATLAB programming for code generation, including the percentage of the win-stay/shift and lose-stay/shift for the macaques performing the acquisition and RL process.

Measurement of cortisol, 5-HT and oxytocin in plasma

The macaques were fasted breakfast in the morning and 1.5 mL blood was quickly collected from the macaque's femoral vein without sedation within a few minutes to minimize effects of the sampling procedure itself on the cortisol level. The cortisol, oxytocin and 5-HT were measured by using QuicKey Pro macaque Cortisol ELISA Kit (Elabscience Biotechnology, E-OSEL-MK0002), Oxytocin ELISA Kit (Elabscience Biotechnology, E-EL-0029) and Serotonin ELISA Kit (Elabscience Biotechnology,E-EL-0033), respectively. Each sample was measured in triplicate repetitions.

Targeted metabolomics

We collected cerebrospinal fluid (CSF) samples from the interspace between the last two lumbar with a sterilized 22-gauge puncture needle in macaques under anesthesia with ketamine (10 mg/kg). The CSF was centrifuged at 4℃, 1489 g for 15 min. The supernatant was immediately collected and stored at −80°C until analysis. Metabolomic analysis of CSF was based on LC/MS. Briefly, the analysis of hydrophilic metabolites and lipids (H650 and HL2400) were performed on a UHPLC system (LC-30AD, Shimadzu) coupled with QTRAP MS (6500+, Sciex) at Shanghai Applied Protein Technology Co., Ltd.. The analytes were separated using a HILIC column (Phenomenex, Luna NH2, 2.0 mm × 100 mm, 3 μm) and a C18 column (Phenomenex, Kinetex C18, 2.1 × 100 mm, 2.6 μm). The measured metabolites were quantified using Multi Quant or Analyst software.

Neuroimaging acquisition and analysis

Macaques were premedicated with atropine (0.05 mg/kg, i.m.) and ketamine (10 mg/kg, i.m.). Anesthesia was maintained with continuous intravenous propofol at 15 mg/kg/h. We monitored end-tidal carbon dioxide (ETCO2) levels and respiratory rates using an MRI-compatible system and covered the animals with a blanket to prevent hypothermia. To ensure a reliable comparison between the SIB and control group, we increased the controls to nine age- and gender-matched healthy macaques.

Using a 3.0 T UMR790 MRI scanner at the KIZ, we obtained MRI, dMRI, and rs-fMRI data. The macaques were under general anesthesia to reduce stress and

motion artifacts, consistent with previous findings that resting-state functional activity persists under anesthesia in both humans and macaques [63, 64].

Structural MRI Data Acquisition

T1-weighted images were acquired using a 3D fast spoiled gradient echo sequence (voxel size = 0.5 mm isotropic, TE = 5.6 ms, TR = 13.01 ms, flip angle = 8°). T2-weighted images were collected with a fast spin echo sequence (voxel size = 0.5 mm isotropic, TE = 396.48 ms, TR = 3400 ms, flip angle = 59°), using a 12-channel head coil.

dMRI Data Acquisition

dMRI parameters included TR = 7740 ms, TE = 90 ms, flip angle = 90°, field of view = 96 mm, matrix size = 96 × 96, and slice thickness = 1 mm, resulting in a voxel resolution of 1 × 1 × 1 mm^3. Diffusion weighting was applied with b-values of 1000 and 2000 s/mm^2 across 64 directions, plus one non-diffusion-weighted image.

Rs-fMRI Data Acquisition

Rs-fMRI images were obtained using an echo-planar imaging sequence with a voxel size of 1.5 mm isotropic, TE of 29 ms, TR of 1700 ms, and a flip angle of 80°. Each session included 500 EPI volumes, with reverse phase encoding data collected to aid in image correction.

Structural MRI Data Analysis

We processed structural data using AFNI [65], FSL [66], ANTs [67], and FreeSurfer [68]. Each animal's T1 image was registered to the NIMH Macaque Template (NMT, version 2.0) [69]. An in-house neural network generated initial skull stripping and WM masks. T2 images were co-registered with T1 using rigid-body transformation, followed by bias correction. A FreeSurfer-based pipeline produced WM and GM surfaces, which were manually reviewed and adjusted for accuracy.

Brain surfaces were segmented into four lobes and 88 regions per hemisphere using CHARM1 and CHARM5 atlases [69]. FreeSurfer extracted GMV for each region. Subcortical regions were parcellated using the SARM atlas [70], covering 13 nuclei like the amygdala and thalamus. Segmentation was done by applying the registration matrix inversely to the SARM atlas. Ventricles were segmented similarly, with manual checks as needed. Volumes of all regions, including ventricles, WM, and subcortical structures, were calculated based on voxel counts.

dMRI Data Analysis

We processed dMRI images using the HCP-NHP diffusion pipeline. Preprocessing included B0 intensity normalization, EPI distortion correction, eddy current and motion correction, and alignment to T1 images. Using MRtrix, we estimated tissue-specific response functions and calculated fiber orientation distributions with the constrained spherical deconvolution model [71]. Fractional anisotropy, axial diffusivity, radial diffusivity, and apparent diffusion coefficient were computed [72]. Probabilistic fiber tractography was performed with MRtrix, using anatomically constrained tractography, with default parameters. Biases were reduced using the SIFT2 algorithm [73]. The brain was parcellated with CHARM5 and SARM atlases. We constructed a weighted 202 × 202 structural connectivity (SC) matrix with MRtrix's tck2connectome, normalizing edge weights using the -scale_invnodevol

option [74]. Connections were validated only if present in all 12 macaques. SC was analyzed at three levels: for the whole brain, it was calculated as the sum of all connections; for each lobe, it was defined as the sum of connection strengths between regions within that lobe; and for individual brain regions, it was measured as the sum of their connection strengths with all other brain regions.

Rs-fMRI Data Analysis

We preprocessed rs-fMRI data using AFNI, following established workflows [75]. The data were divided into five segments of 100 TRs each. The brain was parcellated using CHARM5 and SARM atlases, consistent with structural analysis procedures. Functional connectivity (FC) networks were computed by calculating Pearson's correlation coefficients between mean time series of brain region pairs, forming a 202 × 202 matrix. These matrices were then converted to z-scores using Fisher's z-transformation.

Whole-brain FC was assessed by averaging the lower triangle of the FC matrix, including both positive and negative correlations. For lobe-level analysis, the 202 regions were grouped into lobes and subcortical nuclei for each hemisphere, aggregated into two 5 × 5 matrices. Functional connectivity density (FCD) for each region was calculated by averaging its connections with all other regions, setting negative connections to zero [76].

Network-Based Statistic (NBS) Approach

We used NBS approach to identify clusters of regions with differential FC and SC within intra-hemisphere networks [77]. This non-parametric method controls family-wise errors in multiple comparisons. Connected graph components exceeding thresholds (FC: $t = 3.0$ to 4.0; SC: $t = 2.9$ to 3.5) were tested for significance against a null distribution using permutation testing. The NBS framework enhances statistical power by rejecting the null hypothesis at the component level instead of the individual edge level. Analyses were performed with the NBS toolbox and MATLAB R2021b, and results were visualized with BrainNet Viewer [78].

Administration with ketamine

A low dose of hydrochloric acidulated ketamine (1.0 mg/kg, Jiangsu Zhongmubeikang Pharmaceutical Company) was intramuscularly (i.m.) injected to the two SIB and three control macaques respectively in the morning (divided into four injections with an interval of 10 min, on every Monday and Thursday) [79], total seven × four injections. Blood collection and behavioral tests were conducted prior to and post ketamine administration. The self-injury and control macaques were moved into a novel room with a 24 hr-recording camera in front of each cage, for five days, prior to and post ketamine administration. The wound and neurological function were measured prior to the ketamine administration and post the behavioral test. We also collected plasma in macaques prior to and post the ketamine administration to quantify the levels of cortisol, oxytocin and 5-HT.

Statistical analysis

Behavioral and physiological data was expressed as mean ± standard error of the mean (S.E.M) and analyzed using the GraphPad Prism v8.00 (GraphPad Software, La

Jolla, CA, United States). For physiological and behavioral experiments, Shapiro-Wilk test was used for normality test. Unpaired *t*-test (two-tailed), Analysis of variance (ANOVA) test (with repeated measures where appropriate), or Mann–Whitney U test was applied respectively depending on whether the data were normally distributed or not. Differences were considered significant when $p \leq 0.05$.

For metabolomics data, univariate and multivariate statistical analysis were employed to examine the processed data between the self-injury and control macaques, including principal component analysis (PCA), orthogonal partial least squares discriminant analysis (OPLS-DA), followed by KEGG pathway analysis. Statistical difference was determined using an unpaired *t*-test (two-sample, uncorrected), and $p < 0.05$ indicated statistical significance.

For MRI data analyses to assess the structural differences between SIB and control macaques, we employed Generalized Linear Mixed Models (GLMMs) to analyze measurements at the global, lobe, and region levels, incorporating Hemisphere as a random factor. Importantly, all structural data were adjusted for the intracranial volume of the corresponding hemisphere. For the evaluation of SC differences, Hemisphere was included as a random factor in the GLMM. For the evaluation of FC differences, we analyzed whole-brain FC differences using the GLMM, treating Segment as a random factor. At the lobar and regional levels, we conducted GLMMs with both Segment and Hemisphere included as random factors. Given the relatively small sample size of our study, we have presented both corrected and uncorrected significant results to provide a comprehensive overview of our findings. We note here that all p values are corrected for the number of lobes or regions using the false discovery rate (FDR) method unless specified otherwise.

Supplementary Tables

Table S1. Differential hydrophilic metabolites in CSF

Name	Class	Mass	RT	fold change	p-value
Arachidic Acid	Fatty Acyls	311.3/311.3	12.10	1.0534	0.0351
Chenodeoxycholic acid (CDCA)	Steroids and steroid derivatives	391.4/391.401	9.28	6.1968	0.0450
Deoxycholic acid (DCA)	Steroids and steroid derivatives	391.4/391.402	9.31	2.5292	0.0344
Gluconic acid	Organooxygen compounds	195/129	7.80	0.6600	0.0153
Malic acid	Hydroxy acids and derivatives	133/115.1	8.55	0.8635	0.0350
Maltotriose	Organooxygen compounds	522.2/325.0	8.84	2.3388	0.0456
Myo-inositol	Organooxygen compounds	179/161	7.72	0.6319	0.0051
N-Acetylneuraminic acid	Organooxygen compounds	310.1/121.0	7.75	0.6494	0.0005
Tyrosine	Carboxylic acids and derivatives	182.1/136.1	4.98	0.6732	0.0377

fold change > 1 indicates increased metabolites and < 1 indicates decreased metabolites.

Table S2. Differential lipids in CSF

Name	Class	CalMz	RT	fold change	p-value
PA(18:1/20:1)	Phosphatidic acid	727.5/309.3	5.8	0.8355	0.0315
PC(14:0/20:4)	Phosphatidylcholine	812.5/303.2	5.86	1.3223	0.0085
PC(15:0/18:3)	Phosphatidylcholine	800.5/241.2	5.86	1.2181	0.0110
PC(15:0/22:5)	Phosphatidylcholine	852.6/241.2	5.86	1.1995	0.0137
PS(18:1/18:1)	Phosphatidylserine	786.5/281.2	11.42	1.5596	0.0286
DG(18:2/22:4)	Diacylglycerol	686.6/337.3	5.6	0.6490	0.0496
DG(18:3/20:1)	Diacylglycerol	662.6/335.3	5.65	0.6778	0.0199
DG(19:0/19:0)	Diacylglycerol	670.6/355.3	7	1.3296	0.0334
TG(45:1)-FA16:0	Triglycerides	780.7/507.4	8.41	0.8859	0.0205
TG(45:1)-FA18:1	Triglycerides	780.7/481.4	8.41	0.8817	0.0198
TG(46:3)-FA18:3	Triglycerides	790.7/495.4	7.91	0.7079	0.0437
TG(47:1)-FA18:1	Triglycerides	808.7/509.4	8.71	0.8404	0.0377
TG(48:2)-FA16:0	Triglycerides	820.7/547.4	8.69	0.8246	0.0288
Cer(d18:1/22:1)	Ceramide	620.7/264.4	5.7	0.5407	0.0364

TG(49:3)-FA18:2	Triglycerides	832.8/535.5	8.58	0.8405	0.0039
TG(50:6)-FA20:4	Triglycerides	840.7/519.4	7.73	0.7459	0.0399
TG(51:1)-FA17:0	Triglycerides	864.8/577.5	9.59	0.8826	0.0410
TG(51:5)-FA18:3	Triglycerides	856.8/561.5	8.31	0.7106	0.0280
TG(52:4)-FA20:3	Triglycerides	872.8/549.5	8.87	0.8372	0.0078
TG(53:1)-FA16:0	Triglycerides	892.8/619.5	10.03	0.7107	0.0139
TG(54:5)-FA22:4	Triglycerides	898.8/549.5	8.96	1.3055	0.0366

fold change > 1 indicates increased metabolites and < 1 indicates decreased metabolites.

Table S3. Analysis of KEGG pathway in self-injury macaques

Pathway	**p-value**	**Upregulation or downregulation**
The analysis of hydrophilic metabolites		
carbohydrate digestion and absorption	0.0405	upregulation
bile secretion	0.0089	upregulation
secondary bile acid biosynthesis	0.0013	upregulation
dopaminergic synapse activity	0.0182	downregulation
phosphatidylinositol signaling system	0.0434	downregulation
melanogenesis	0.0091	downregulation
prolactin signaling	0.0167	downregulation
taste transduction	0.0478	downregulation
glucagon signaling	0.0390	downregulation
pyruvate metabolism	0.0463	downregulation
citrate cycle	0.0301	downregulation
methane metabolism	0.0071	downregulation
carbon metabolism	0.0122	downregulation
The analysis of lipids		
alpha-linolenic acid metabolism	0.0439	upregulation
linoleic acid metabolism	0.0282	upregulation
metabolism of glycine,serine, and threonine	0.0498	upregulation
phosphatidylinositol signaling system	0.0291	downregulation
sphingolipid metabolism	0.0252	downregulation
necroptosis	0.0101	downregulation
The following pathway changes were not significant		
glycerophospholipid metabolism	ns	upregulation
retrograde endocannabinoid signaling	ns	upregulation
neurotrophin signaling	ns	downregulation

cAMP signaling	ns	downregulation
sphingolipid signaling	ns	downregulation
phospholipase D signaling	ns	downregulation
glycerolipid metabolism	ns	downregulation
FcγR-mediated phagocytosis	ns	downregulation
adipocytokine signaling	ns	downregulation
GnRH signaling	ns	downregulation
fat digestion and absorption	ns	downregulation

Table S4. The abbreviation and region name of the brain areas in the figures of neuroimaging results

Abbreviation	Region Name
Acb	accumbens
AI	primary auditory cortex
AIP	anterior intraparietal area
AL/RTL	rostral areas of the lateral belt
Amy	amygdala
ant STSf	anterior fundus of the superior temporal sulcus
ant TE	anterior area TE
area 10	frontal pole
area 11	area 11
area 12m/o	medial and orbital area 12
area 12r/l	rostral and lateral area 12
area 13	area 13
area 14	gyrus rectus
area 23	area 23
area 24a/b	areas 24a and 24b
area 24a/b prime	areas 24a' and 24b'
area 24c	area 24c
area 24c prime	area 24c'
area 25	subgenual cortex
area 29	area 29
area 30	area 30
area 31	area 31
area 32	area 32
area 35	area 35
area 36	area 36
area 3a/b	areas 3a and 3b
area 44	area 44
area 45	area 45

area 46d	dorsal area 46
area 46v/f	ventral and fundus portion of area 46
area 5d	dorsal area 5
area 7a/b	inferior parietal lobule areas 7a and 7b
area 7m	area 7 (PGm) on the medial wall
area 7op	parietal operculum
area 8A	periarcuate area 8A (frontal eye fields)
area 8B	area 8B
area 9	area 9
area v23	area v23
areas 1-2	areas 1-2
caudal ERh	caudal entorhinal cortex
Cd	caudate
CL/ML	caudal areas of the lateral belt
CM	caudomedial belt region
EpiThal	epithalamus
Fro	frontal lobe
Fro-Sub	frontal-subcortical
FST	the floor of the superior temporal area
fundus IPS	fundus of the intraparietal sulcus
G	gustatory cortex
HF	hippocampal formation
Hy	hypothalamus
Iam/Iapm	medial agranular insular region
Ins	insula
lat Ia	lateral agranular insular region
LIP	lateral intraparietal area
LOP	lateral occipital parietal area
LVPal	lateral and ventral pallium
M1	primary motor cortex
Mid	midbrain
mid ERh	middle entorhinal cortex
MIP	medial intraparietal area
MST	medial superior temporal area
MT	middle temporal area
Occ	occipital lobe
OLF	primary olfactory cortex
Par	parietal lobe
parabelt	parabelt areas of auditory cortex
Par-Occ	parietal-occipital
Pd	pallidum

PEa	area PEa
Pi	parainsula
PMd	dorsal premotor cortex
PMv	ventral premotor cortex
post TE	posterior area TE
PrCO	precentral operular area
preSMA	presupplementary motor area
PreThal	prethalamus
PrT	Pretectum
Pu	putamen
R/RT	rostral areas of the core
Ri	retroinsula
RM/RTM	rostral areas of the medial belt
rostral ERh	rostral entorhinal cortex
RTp	polar rostrotemporal cortex
SII	secondary somatosensory cortex
SMA	supplementary motor area
STGr	rostral superior temporal gyrus
Sub	subcortical
TAa	area TAa
TE in STSv	area TE in the ventral STS
Tem	temporal lobe
TEO	area TEO
TF/TFO	areas TF and TFO
TGa	agranular temporal pole
TGd	dysgranular temporal pole
TGg	granular temporal pole
TH	area TH
Thal	thalamus
TPO	temporal parietooccipital associated area
Tpt	temporo-parietal area
V1	primary visual cortex
V2	visual area 2
V3d/V3A	visual areas V3d and V3A
V3v	ventral visual area 3
V4d	dorsal visual area 4
V6	visual area V6
V6A	visual area V6A

Supplementary Figure 1

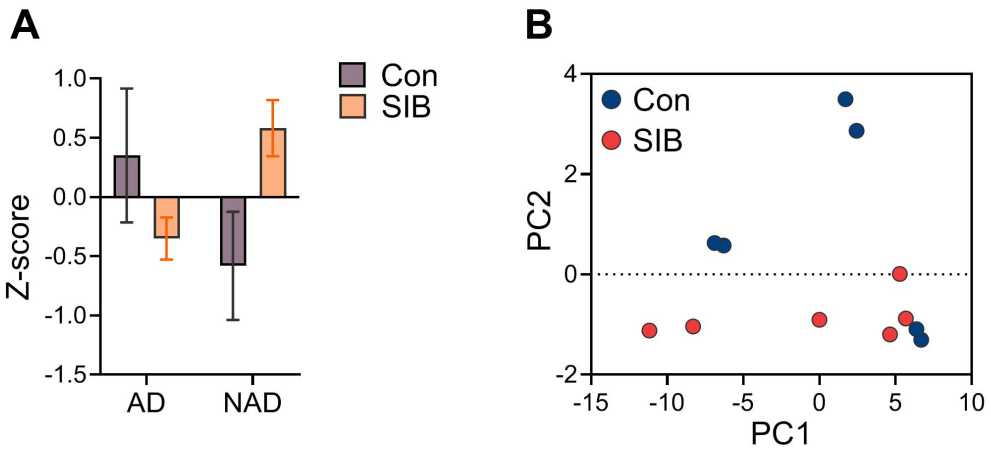

Figure S1. Spontaneous behavior in macaques.

A: Self-injury macaques showed overall low apparent displacement (AD) and high non-apparent displacement (NAD) when compared with the controls.

B: Principal component analysis (PCA) of kinematic parameters between self-injury macaques and control animals.

Supplementary Figure 2

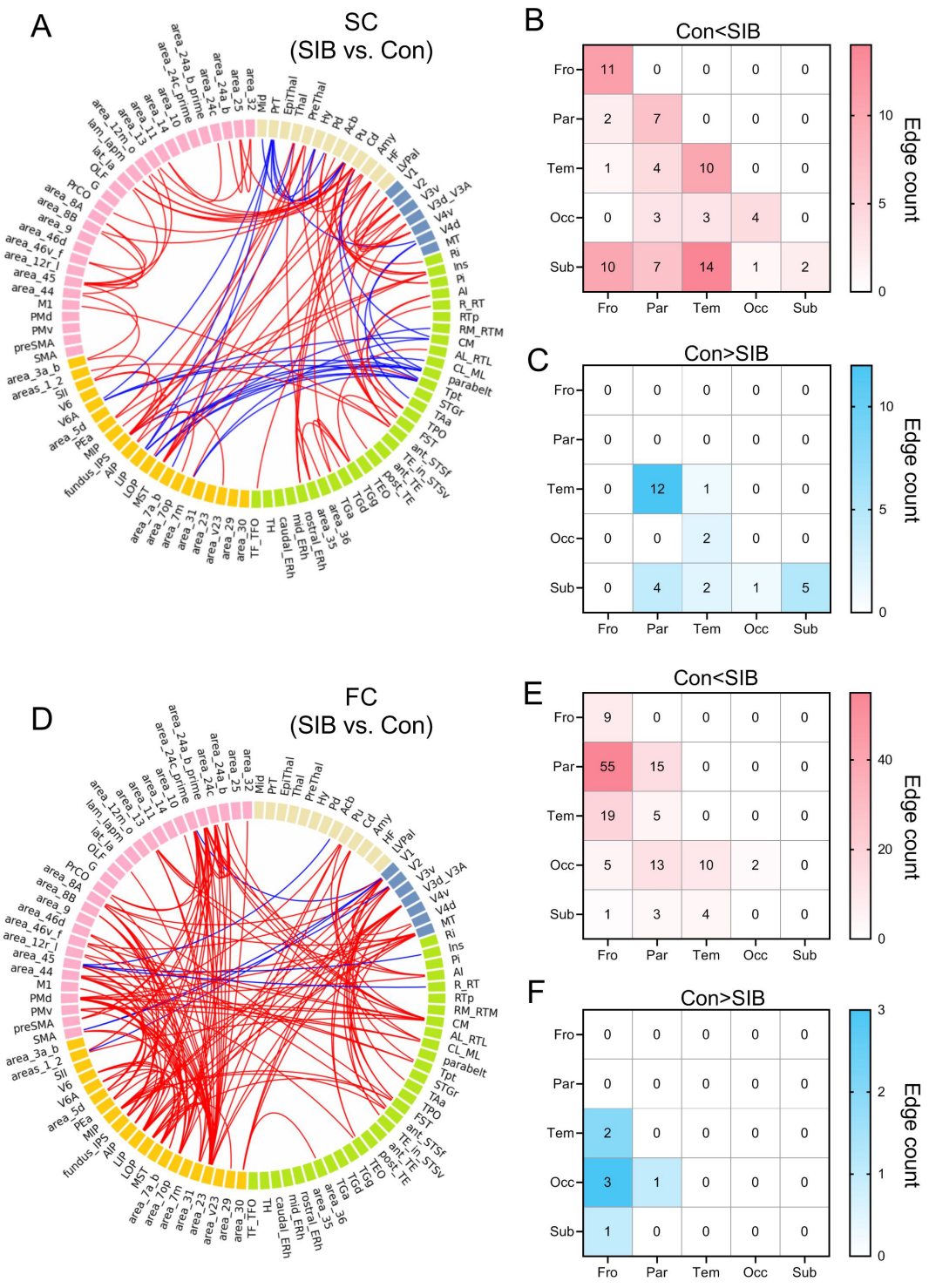

Figure S2. NBS results of structural and functional connectivity

A & D: Visualization of structural (A) and functional (D) connectivity changes, with decreases shown in blue and increases in red, in self-injury macaques (SIB) compared with controls (threshold of FC: t = 4.0; threshold of SC: t = 2.9). B-C: Heatmaps showing the number of increased (B) and decreased (C) structural connectivity

instances in self-injury macaques compared with controls at the threshold of t = 2.9. Fro - frontal lobe; Par - parietal lobe; Tem - temporal lobe; Occ - occipital lobe; Sub - subcortical area.
E-F: Heatmaps depicting the number of increased (E) and decreased (F) functional connectivity instances in self-injury macaques compared with controls at the threshold of t = 4.

Legends for movie S1 to S2

Movie S1 showed a self-injury macaque quietly biting its arm.

Movie S2 showed a self-injury macaque biting its lower limbs engaging in stereotypical behavior.